LEBANESE AMERICAN UNIVERSITY

3D Printing of IPMC Actuators Based on the Direct Assembly Method

By

Serge Sarkis

A thesis
submitted in partial fulfillment of the requirements
for the degree of Master of Science in Mechanical engineering

School of Engineering
December 2022

LAU
الجامعة اللبنانية الأميركية
Lebanese American University

THESIS APPROVAL FORM

Student Name: Serge Sarkis I.D. #: 202005003

Thesis Title : 3D Printing of IPMC Actuators Based on the Direct Assembly Method

Program: Master of Science in Mechanical engineering

Department: Mechanical engineering

School: Engineering

The undersigned certify that they have examined the final electronic copy of this thesis and approved it in Partial Fulfillment of the requirements for the degree of:

Masters of Science in the major of Mechanical Engineering

Thesis Advisor's Name Barbar Akle	Signature [redacted]	DATE: Dec 15, 2022 (Day Month Year)
Thesis Co-advisor's Name Ali Ammouri	Signature [redacted]	DATE: Dec 16, 2022 (Day Month Year)
Committee Member's Name Evan Fakhoury	Signature [redacted]	DATE: Dec 16, 2022 / (Day Month Year)
Committee Member's Name Charbel Tawk	Signature [redacted]	DATE: 16/12/2022 / (Day Month Year)

LAU
الجامعة اللبنانية الأميركية
Lebanese American University

THESIS COPYRIGHT RELEASE FORM

LEBANESE AMERICAN UNIVERSITY NON-EXCLUSIVE DISTRIBUTION LICENSE

By signing and submitting this license, you (the author(s) or copyright owner) grants the Lebanese American University (LAU) the non-exclusive right to reproduce, translate (as defined below), and/or distribute your submission (including the abstract) worldwide in print and electronic formats and in any medium, including but not limited to audio or video. You agree that LAU may, without changing the content, translate the submission to any medium or format for the purpose of preservation. You also agree that LAU may keep more than one copy of this submission for purposes of security, backup and preservation. You represent that the submission is your original work, and that you have the right to grant the rights contained in this license. You also represent that your submission does not, to the best of your knowledge, infringe upon anyone's copyright. If the submission contains material for which you do not hold copyright, you represent that you have obtained the unrestricted permission of the copyright owner to grant LAU the rights required by this license, and that such third-party owned material is clearly identified and acknowledged within the text or content of the submission. IF THE SUBMISSION IS BASED UPON WORK THAT HAS BEEN SPONSORED OR SUPPORTED BY AN AGENCY OR ORGANIZATION OTHER THAN LAU, YOU REPRESENT THAT YOU HAVE FULFILLED ANY RIGHT OF REVIEW OR OTHER OBLIGATIONS REQUIRED BY SUCH CONTRACT OR AGREEMENT. LAU will clearly identify your name(s) as the author(s) or owner(s) of the submission, and will not make any alteration, other than as allowed by this license, to your submission.

Name: Serge Sarkis

Signatur[redacted]

Date: 19-12-2022

PLAGIARISM POLICY COMPLIANCE STATEMENT

I certify that:

1. I have read and understood LAU's Plagiarism Policy.
2. I understand that failure to comply with this Policy can lead to academic and disciplinary actions against me.
3. This work is substantially my own, and to the extent that any part of this work is not my own I have indicated that by acknowledging its sources.

Name: Serge Sarkis

Signature: [redacted] Date: 19 / 12 / 2022
Day Month Year

ACKNOWLEDGMENT

This project would not have been possible without the support of many people.

Many thanks to my advisors, Dr.Barbar Akle and Dr.Ali Ammouri for providing endless support and guidance.

I would like to also thank Ms. Nicole Jureidini, Mr.Salim Jamal-Eddine, Mr.Elias Mouarbes, Mr. Elie Abi Aad , Ms. Rana EL-Ghorayeb and all LAU staff members for their help and assistance throughout my experiments.

I would like to thank my colleague Zeina Gerges for her support and companionship during this journey.

Finally, many thanks to my family and friends who endured this process with me and provided me with endless love and support

3D Printing of IPMC Actuators Based on the Direct Assembly Method

Serge Sarkis

ABSTRACT

Ionic polymer metal composites are a type of electroactive polymers, they are composed of an ionomer membrane sandwiched between two conducting high surface area electrodes. They act as an actuator under the application of a relatively small applied electric voltage in the order of 1 to 4V, producing large strains compared to other actuators. The middle membrane acts as an eclectic insulator that allows ions to move from one electrode to the other. The negatively charged high surface area electrode attracts the positively charged mobile cations resulting in actuation. IPMCs also operate in sensing mode by generating electricity when subject to mechanical deformations. This versatility in operation makes them good candidates for a number of complex applications including biomimetics, micro-robotics, and medical catheters. These different application demand complex geometries and high level of performance. The electrode morphology has been proven to play a critical role in the performance of IPMCs. In this thesis, the process of 3D printing the IPMC along with the electrodes using FDM 3D printing is investigated. Our method will enable the 3D printing of both:

the Nafion insulating center layer, and a Ruthenium Dioxide-Nafion mixture composing the high surface area electrode. The electrodes performance will be evaluated against the traditional impregnation reduction method for electrode plating applied to a 3D printed membrane. Also, the performance of a membrane made by hot-pressing Nafion pellets, a traditional Nafion membrane fabrication method, will be used to validate the 3D printing process. The 3D printed electrodes achieved a strain of 3.71E-4 which was lower than the strain of impregnation reduction method at 1.14 E-3. This was attributed to excessive flaking and poor mixing of the Ruthenium Dioxide particles in the polymer matrix.

Keywords*:* IPMCs, FDM, 3D printing, Impregnation/reduction electrode morphology, Nafion, Polymer metal mixture.

TABLE OF CONTENTS

ACKNOWLEDGMENT V

ABSTRACT VI

TABLE OF CONTENTS VIII

LIST OF TABLES X

LIST OF FIGURES XI

I-INTRODUCTION 1

II-LITERATURE REVIEW 5

2.1 IPMC Actuation Process 5

2.2. Fabrication Methods for Nafion Membranes 6

2.3. IPMC Electrodes 11
2.3.1. Electrode Morphology 11
2.3.2. Electrode Fabrication Methods 13

2.4. Nafion Properties 17
2.4.1. Thermal Properties 17
2.4.2. Chemical Treatment 20

2.5. Die Swell 20

2.6. 3D Printing 23
2.6.1. 3D Printing Issues 26
2.6.2. Bed Adhesion 27

2.7. Polymer Metal Composites 28
2.7.1. Polymer Metal Mixing 28
2.7.2. Polymer-Metal 3D Printing 31
2.7.3. Characteristics Polymer Metal Mix 31

2.8. Filament Making ... 32

III-METHODOLOGY ... 34

3.1. Instrumentation and thermal sensors ... 34

3.2. Flow of Nafion precursor ... 36

3.3. Membrane preparation ... 37
3.3.1. Hot pressed membranes ... 37
3.3.2. 3D printer set up ... 38
3.3.3. 3D printing process ... 44
3.3.4. Filament Fabrication methods ... 44
3.3.5. Chemical activation of 3D printed samples ... 55

IV-RESULTS AND DISCUSSIONS ... 58

4.1. Extrusion process ... 58

4.2. DAP mixing and polymer-metal filament extrusion ... 58

4.3. 3D printed samples ... 70

4.4. Rheology simulation ... 75

4.5. Chemical activation ... 77

4.6. Hot pressed membranes ... 80

4.7. Polymer-metal mixing ... 83

4.8. Actuation results ... 86

V-CONCLUSION ... 96

VI-FUTURE WORK ... 97

REFERENCES ... 98

LIST OF TABLES

Table 1-Results of 4 wire kelvin test 51
Table 2-Quantities required for polymer-metal mixture 60
Table 3-Plating progress of reference 3D printed membrane 78
Table 4-Plating progress of ruthenium 3D printed membrane 79
Table 5-Displacement results 92
Table 6-Specifc capacity results 94

LIST OF FIGURES

Figure 1-Increase in stiffness with different number of plating cycles courtesy of [21] .. 15
Figure 2-Curve fitting of PT100 data 34
Figure 3-Wheatstone bridge arrangement 35
Figure 4-Extrusion system........ 47
Figure 5-Plunger head design........ 48
Figure 6-Thermal Mold 49
Figure 7- 4-wire kelvin test configuration........ 52
Figure 8-Variation of viscosity in function of temperature taken from [59]........ 61
Figure 9-NTC 3950 100k thermistor temperature measurements........ 62
Figure 10 -Nafion/Ruthenium Dioxide mixture 63
Figure 11-variation of extruder temperature with respect to time........ 65
Figure 12-Variation of plate temperature with respect to time 67
Figure 13-Variation of thermal mold temperature with respect to time........ 67
Figure 14-Variation of plunger temperature with respect to time........ 69
Figure 15-Variation of plate temperature with respect to time 70
Figure 16-Membrane 1 71
Figure 17-Membrane 2 72
Figure 18-Simulation of Nafion membrane on heat bed........ 74
Figure 19-Pla membrane surface temperature........ 75
Figure 20-Results of numerical optimization for mobility factor 76
Figure 21-Temperature profile from the Polyflow simulation........ 77
Figure 22-surface resistance measurement for second electrode side........ 79
Figure 23-Nafion membrane before cutting........ 81

Figure 24-Nafion membrane with hot pressed Ruthenium Dioxide electrodes before cutting 82
Figure 25-Ruthenium Dioxide electrode- smooth surface 84
Figure 26- Ruthenium Dioxide-electrode with scrapped surface 84
Figure 27-Damaged electrode from hot pressed sample 85
Figure 28-Filament cross-section 86
Figure 29-Actuation schematic diagram 87
Figure 30-Control circuit 88
Figure 31-Voltage amplifier 88
Figure 32-response of 3D printed sample with impregnation-reduction plating 90
Figure 33-response of 3D printed sample with Ruthenium Dioxide electrode 91
Figure 34-Response of hot-pressed sample 92

CHAPTER ONE

INTRODUCTION

Smart materials are special materials that produces a useful response when subject to an external stimulus [1-4]. While most of the materials respond to an external stimulus, as for example the change of volume due to temperature, smart materials respond with what is referred to as “meaningful” engineering response. Some of these materials can even work interchangeably in sensing and actuation. Smart materials are thus materials that can be used in multiple fields of operation: Shape changing, Self-actuating, Self-sensing, Self-diagnostic and Self-healing [5-7].

There are multiple types of smart materials, they differ by their areas of applications depending on the mode of energy transfer in the response they produce.

Electro active polymers (EAPs) exhibit an actuation response when subjected to an electrical stimulus and in some cases produces an electrical response to a mechanical deformation [8,9]. They are divided into two groups: electronic EAPs and Ionic EAPs due to different working mechanisms. The former is based on the movement of electrons inducing electric fields or Coulombic forces. Electronic EAPs produce fast responses and has a high energy density [10]. However, Ionic EAPs actuate based on ionic diffusion, resulting in a slower response that is limited by the diffusion rates of the mobile ions. There main advantage is that they require a lower activation voltage (1-5 V) compared to the electronic type EAPs and most of them produce larger deformations [11].

This electromechanical response made EAPs, especially Ionic EAPs, a popular choice of actuator for “artificial muscles” since they operate at lower voltages that are safe for in-vivo actuation while generating displacement and force profiles comparable to that in animal muscles. [6,11].

Ionic polymer metal composites (IPMCs) are a subgroup of Ionic EAPs that has reaped a lot of success in this domain. What sets it apart from other ionic EAPs is that it has a relatively faster response and they can be built to either operate in aqueous mediums or in air and vacuum [12,13]. They have been used extensively in biomimetic applications such as the work on the movement of a robotic jelly fish and a robotic fish in [14-16]. Other fields of operation include energy harvesting [17], biomedical applications as catheters [18] or as sensors [12]

An IPMC has mainly three components: A polyelectrolyte membrane solvated with an appropriate electrolyte fluid and sandwiched between two conducting high surface area electrodes. Varying the characteristics of any of the components affects the response of the transducer.

Conventionally, the electrodes are formed by the chemical deposition of metal particles on the outer surface of the membrane. This method suffers from low reliability and lack of control over the electrode morphologies. The direct assembly method was developed in [19] enabling more control over the electrode characteristic and providing a significant improvement in response. This is done by painting or spraying a conductive metal/polymer mixture directly on the membrane. From a practical point of view, it allows the user to mechanically place the electrodes, the material species composition and distribution, quantity dispersed and dimension. Painting and spraying however does not provide small resolutions and an alternative more precise dispersion method can add to the efficiency of this method.

As for the membranes, actuators were commonly built using thin Nafion membranes (approximately 200μm) obtained from Dupont. Therefore, the actuators formed were limited to standards shapes and complex applications required integrating multiple IPMC actuators together which is costly, less reliable, complex to assemble. In order to extend the range of possible shapes, different manufacturing processes have been studied. Recently, a study conducted by [20] produced IPMC actuators by 3D printing the Nafion membrane. This method provides flexibility in manufacturing by enabling the production of complex monolithic shapes with great accuracy. The author however used the chemical electroless process to form the electrodes. There is still room for improvement, choosing the location and thickness of the electrodes would allow the user to exploit the complex geometry and control the 3D motion of the actuator.

According to our knowledge, there are no existing studies involving the usage of both 3D printing and DAP combined. In this work, the advantage and practicality of combining these two processes is investigated. An IPMC actuator will be produced by 3D printing both the polyelectrolyte membrane and the high surface area electrodes. Together, they can provide more flexibility in the design and assembly of the IPMC actuators, improve the precision and control the 3D movement of manufactured 3D shaped.

In addition to the novel IPMC, a Nafion membrane will be 3D printed and electrodes will be plated using the impregnation-reduction method. Investigating the performance of the two samples would allow us to:

- Validate the 3D printing process by comparing the results obtained to the ones in [20]
- Asses the performance of the electrodes using the new method compared to the traditional impregnation-redox method

A third Nafion membrane will be made by hot-pressing multiple Nafion precursor pellets using a hot-press machine. The electrodes will also be made using the impregnation-redox method. The performance of the resulting sample will provide a benchmark for the previous methods.

To test the actuation of the produced membranes, a step voltage of 2 volts is applied for a short duration (1-10 seconds). The membranes are placed in a cantilever configuration and connected to a control circuit. The resulting displacement is measured using a laser displacement sensor. The current passing through the circuit is also measured to calculate the specific charge of each membrane.

The remainder of the thesis is divided into the following structure: a literature review of the different topics in this study is presented in Chapter 2. The methodology applied in each step of the fabrication process is discussed in Chapter 3 followed by an interpretation of the obtained results in Chapter 4. The conclusion of the study along with suggested ideas for future research are presented in Chapter 5

CHAPTER TWO

LITERATURE REVIEW

As mentioned before, each component in the IPMC actuator plays a key role in the overall performance. In this section, a brief overview will be presented on each part while highlighting the characteristics and important factors that need to be considered during the experimental process of this study

2.1 IPMC Actuation Process

The actuation process, mainly bending, is based on electro-osmosis [21]. Under the application of an electric field, cation will migrate towards the negative electrode and drag along some water molecules. High concentration of charge on one side will trigger an osmosis event where additional water molecule will defuse towards the negative electrode. This will lead to an increase in actuation and bending towards the anode.

Diving deeper into the matter, the hydration of the moving cation was found to play a crucial role in the actuation and output response [22]. [23] investigated the usage of different cations on the performance of the IPMC. It was found that the cation with the largest hydration shell produced the highest output force. The results were found to be in terms of force produced:

$Li^+ > Na^+ > (K^+, Ca^{++}, Mg^{++}, \text{and } Ba^{++}) > (H^+, \text{TBA, and TMA})$

A larger hydration shell means more viscous drag between the molecule as they are moving. Unsurprisingly, the cations with the largest hydration shell also had the slowest response. The result ranked in terms of ion mobility:

$u[Li^+] < u[Na^+] < u[K^+])$

Different types of response can be achieved in IPMC going beyond the cantilever configuration. This however will require using pattern electrodes and a different geometry of the membrane overall.[24] used multiple IPMCs in rectangular shape and placed them in a soft booth in the shape of an underwater fin. By using different activation patterns, they were to create twisting motion and obtained a lift to drag ratio of 6.7. The result is promising an highlights the potential of a patterned configuration. The structure is however bulky and can be further improved without having to use multiple IPMC but one monolithic structure capable of multi degree of freedom motion. the study in [25] investigated the 2D motion of a cylinder IPMC tube with 4 separated electrodes. They extruded a cylinder with flanges and removed the flanges to have 4 separated electrodes once the plating was finished. Expanding on the concept of cylinder tubing, the study in [26] used a similar configuration to make a slender tube IPMC. The tube was hollow on the inside and this led to deformation of the geometry due to rearrangements of the cations. This highlights the effect of actuator geometry on the response.

2.2.Fabrication Methods for Nafion Membranes

Nafion membranes are available in the form of thin sheets that can be purchased directly off the shelf. However, due to the recent advances and the different applications of IPMCs, thicker and more complex shapes are required. This led researchers to investigate different manufacturing processes to achieve this aim.

[27] successfully obtained Nafion membranes via solution casting. They used the liquid dispersion form of Nafion for that end. The process although reliable requires a large amount of dispersion (8-9 times the amount of Nafion film required). [28] achieved

the same process but by dissolving Nafion film using an appropriate solvent. Study in [21] were able to achieve thick IPMC with hot pressing instead of solution casting. In their work, they hot pressed multiple ready-made Nafion films into a single membrane and applied the impregnation-reduction plating method to form a single actuator. The Nafion films were left at 180°C temperature for 20 min before being pressed at 180°C for 10 min under a 50 Mpa pressure. Multiple samples were made by pressing together an increasing number of Nafion films (from 3 to 5). Tip displacement and force generated were investigated for different voltage values. For all applied voltages, a decrease in generated distance was observed with increase in membrane thickness (number of hot-pressed films) but produced a higher tip force. All tests were conducted with water hydrated samples

[29] produced thick membranes by using spray painting from Nafion dispersion as well. A 5% wt. Nafion® water dispersion (1100 EW) from DuPont and an airbrush (Master Airbrush Model G22) were used. The method consists of spraying the dispersion directly onto an ABS weighing dish, wish makes it easier for the Nafion membrane to peel off once it is dried out. Custom shapes can be created by each will require a different mold. The lack of high temperature is convenient however the thickness produced per spraying cycle depends on the type of brush. It was approximated that 100 microns were deposited per cycle. It was also required that each deposited layer dries out before spraying in order to avoid tearing or bubble formation. Dynamic Mechanical Analysis (DMA) at different frequencies showed that the painted Nafion membrane had a slightly

higher modulus of elasticity compared to the Nafion N117 from Dupont. This was attributed to painted membrane having a more crystalline structure.

Extrusion of the films is possible as the work in [25] demonstrated. In this case, Nafion in the precursor form is used as it is required to be melt processable unlike the activated Nafion films [30]. The resulting film should be chemically activated afterwards. Also, extrusion introduces an additional issue which is the phenomena of die swell. As noted in [31] the die orifice was found by trial and error as the precursor Nafion would swell and expand in size afterwards. A die swell ratio of 1.71 was achieved which is significant in case of very precise applications. Also, a high pressure was needed for extrusion, this is due to the thermal properties of Nafion that will be discussed later. The temperature required to achieve good flow was around 220 °C. The author also noted that Nafion should be extruded directly and at once, without long residence times in the extruder due to thermal degradation. The products would start to turn brown and contaminate the produced samples. [32] used DMF (dimethylformamide) as a plasticizer to extruder Nafion and Aquivion films. Extrusion was achieved using a single screw extruder and at 100°C. Lower temperature is needed in order to avoid boiling of the DMF. The resulting membranes were compared to the N117 Nafion membrane from Dupont. The resulting ionic conductivity and water absorption was larger for the extruded Nafion/DMF films and Aquivion/DMF films compared to the N117 membranes. In order to remove the DMF plasticizer, the extruded membrane were subject to annealing. The measured stiffness of an extruded membrane after annealing for a 50/50 Nafion-DMF blend was 160 MPa which is lower than that of Nafion (around 289 MPa at 50% humidity [29])

Injection molding can also be used and was applied in [31] but used a higher temperature of 250°C. Again, temperature and pressure were found by trial and error in this case. Interestingly, the resulting membranes from extrusion and injection molding had different stiffnesses, 2.5 Mpa and 3 Mpa respectively. Based on those results and the ones of [29], it seems the type of manufacturing process can affect the response depending on the alteration of the crystalline structure.

In any of the above-mentioned methods, the cooling response should be considered carefully. [31] mentioned in their work that rapid cooling or induced layering due to cooling gradients result in failure at the reduction stage and possible poor performance due to added boundaries and layers that hinder ionic motion. This was mostly noticeable in the injection molding process

Thick membranes are attractive for some applications as they produce large forces but also lead to a reduction in strain [33]. They found an approximately linear decrease in elastic modulus and a quadratic increase of bending stiffness with increase of membrane thickness.

There is also the possibility to fabricate membranes using 3D printing such as in [14,20]. In [34], 3D printing capabilities of Nafion and Aquivion were investigated. Extrusion was achieved at a temperature of 230°C for Nafion filament but later 260°C when 3D printing. The Noztek Pro was used as an extruded which is an off the shelf single screw extruder. The advantages of 3D printing are the formation of a monolithic structure instead of combining multiple IPMC actuators, and being limited to standard shapes from injection molding or ready-made membranes. The complexity of the shapes that can be obtained from 3D printing enables more complex multi degree of freedom motion

Although the 3D printing process is very attractive and promising, it still suffers from multiple draw backs. Mainly, Nafion precursor filaments are very flexible with elastic modulus of 2.5 Mpa as reported previously in [31] and 3.76 Mpa reported in [34]. For comparison, the NinjaFlex filament which is one of the most flexible material found in the market is around 12 Mpa. The printers are expected to be fitted with the proper upgrades and the print settings should be varied to achieve a successful print. [35] mention reaching temperature of 260°C for the extrusion head and 180 °C bed temperature, covered with double sided Kapton tape, to obtain good bed adhesion. Low speeds of 5 mm/s for printing were used along with 120% flow rate, 100% infill density and 60% overlap to guarantee a good structure. To solve the different temperature and flexibility issues, they used two types of 3D printers: the Raised 3D N2 Plus and Lulzbot Mini with the latter fitted with the Flexystruder specifically designed to print flexible filaments. In a later publication, the author mentions that the optimal temperature to successfully 3D print Nafion was around 290°C.[29]

An important note was mentioned when dealing with Nafion precursor in [35], the pellets should avoid any moisture in order to avoid any partial hydrolysis. This could be achieved by either using appropriate desiccants or heating the pellets at 105°C for 20 hours. [36] and [20] also mentioned the possibility of obtaining HF gases during melting of the pellets which is highly toxic. [36] mentions that although traces of HF gases can be detected, especially when the polymer starts degrading, the appropriate precautions should always be used when melting the precursors.

2.3. IPMC Electrodes

The electrodes placed on either side of an IPMC are responsible for distributing the electric field produced when a voltage is applied on them and forcing the mobile ions to move and form an electric double layer. They will also generate a potential when the actuator is used in sensing mode. Multiple materials were investigated such as palladium, silver, copper, nickel, carbon black, carbon nano-tubes, and many others [37, 38] as conducting metal and non-metals [39]. Conventionally, platinum or gold are usually used due to their low surface resistivity and good chemical stability [40]

An overview of the different electrode characteristics that affect performance will be covered first. Then, the different manufacturing techniques available will be discussed with reference to their ability in controlling or improving the aforementioned characteristics.

2.3.1. Electrode Morphology

The electrode morphology was investigated thoroughly in literature. There are some key characteristics that were found to have direct influence on the performance of the IPMC actuator.

[41] found in their study that the actuation strain per unit voltage increases with each layer of platinum applied until the electrode stiffness starts to hinder the actuation process. In other words, the thickness of the electrode was found to increase strain up to a certain limit. [42] found that the increase of depth and uniformity of the electrode improves the performance of the transducer. Their modeling results along with the

findings of [43] highlight the importance of the boundary layer between the electrode and the polymer used.

Experiments conducted in [19] showed that the strain output increased with capacitance of the actuator. In this case, ruthenium dioxide was used instead of platinum as it provided more capacitance. Additionally, increasing the thickness of the electrode was found to increase the displacement and strain output. On the other hand, decreasing the ionomer membrane thickness was found to decrease the micro strain slightly and increase the displacement.

[44] studied the electromechanical response of three different ionomers. They did not find a strong correlation between performance (block force, strain output) and ionic exchange capacity or conductivity of the polymer. Instead, a strong correlation was found between the capacitance measured and transducer response. Concretely, they found a linear relationship between capacitance and strain output at each frequency tested. Since the different ionomers were used, it was concluded that the accumulation of charge on the polymer-metal interface has a strong effect on strain produced.

Furthermore, the results in [45] showed that the peak response increased proportionally with the increase of electrode thickness. However, a thicker electrode means a slower response since the ions would take more time to diffuse into the electrode. They also showed that the capacitance increases proportionally to the thickness of the electrode.

Good surface conductivity is required for the transducer to perform adequately. It is known that surface resistivity plays a crucial role in the IPMC actuation [46]. One interesting result was mentioned in [21] where they found that the increase in surface resistance of the actuator was linearly correlated with the increase of distance from the tip.

There is no evidence that this will hold when using different manufacturing methods to fabricate the electrodes.

It is also reported that IPMC suffer from water leakage from there electrodes when operated in air [47]

In summary, having a uniform electrode with high capacitance, a reasonable thickness and a low surface resistivity is required. Good adhesion with the polymer is a must to ensure ionic conductivity in the boundary layer interface

2.3.2. Electrode Fabrication Methods

The most common method used for the fabrication of electrodes on an IPMC is the impregnation-reduction method or electroless plating [48]. In this process, the membrane or actuator is placed in a metallic solution, such as 0.01 M $PT(NH_3)_2CL_2$ [49], to saturate it with metallic ions. After that, a reducing agent is applied to reduce the metallic ions into metal particles. An important aspect of this method is the concentration of the reducing agent applied, the time delay between each increase in concentration and the number of plated layers. [49] uses 0.05 %w/w of $NaBH_4$ for Nafion and the same quantity is added every 30min. The process proceeds inwards and at a slow rate. Gold electroplating can be also applied to reduce the surface resistance and improve performance.

The concentration should not be increased rapidly, since high concentrations will lead to rapid reduction of platinum ions on the surface which in turn will reduce the penetration of platinum into the membrane and decrease the performance of the actuator [44].

An optional step would be to perform an ion exchange at the end [49]. The cation used in the solution plays a role in the IPMC performance as discussed previously.

This method, although reliable and very practical, provides little control over the electrode morphology and the key factors needed to optimize the actuation process. Electroless plating provides only an indirect and non-repeatable way of varying the electrode thickness which is to vary the reducing agent concentration. In addition, it is showing low repeatability in terms of resulting performance when manufacturing multiple transducers as mentioned in [14]. In a bid to investigate the electromechanical coupling of IPMC actuators and their ionic conductivity, a series of actuation experiments were conducted in [44] on different ionic polymer membranes: Nafion, BPSH (sulfonated poly(arylene ether sulfone)) and PATS (poly(arylene thioether sulfone)). During electrode plating, they note that different concentrations of reducing agents are needed and provide optimal concentrations for each membrane based on type and thickness. The same concentration applied to Nafion were applied to BPSH 35(the number of sulfonic acid groups connected to the polymer backbone) and resulted in rapid reduction of the platinum on the surface and poor penetration into the membrane. A last note to mention is that the impregnation-reduction technique cannot incorporate non-metallic materials such as carbon nanotubes that can provide additional benefits such as high surface area conduction.

It was mentioned in [21] that the usage of a single layer of platinum by electroless plating results in a poor resistivity and unreliable performance. One solution to that would be to repeat the process multiple times as mentioned in [23,50] until getting the result required. This is however accompanied by an uncontrolled increase in the thickness of the electrode and as a result a decrease in performance in terms of displacement. The multiple plating results in [21] showed a noticeable increase in stiffness of the IPMC actuator with each number of plating cycles. The numerical values are shown in figure.1 below:

Figure 1-Increase in stiffness with different number of plating cycles courtesy of [21]

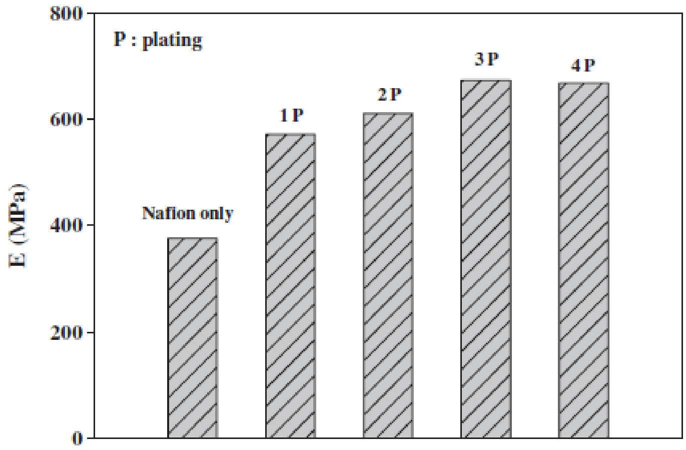

All values are reported for a Nafion membrane made of 5 stacked films.

There have been numerous variations adapted to the impregnation redox method to improve the performance of the transducer. [51] hot pressed different metals such as palladium, silver or graphite directly on the surface and the impregnation method was applied after that. [28] Suggested, without application, casting Nafion membrane and casting on top a solution of ionomer-metal mix.

[52] obtained nano dispersed electrodes by electroless plating using alcohols, the resulting electrodes were thicker but did not increase the thickness drastically. This method results in high capacitance but does not allow a control of the thickness. In a similar approach, [35] used Polyvinylpyrrolidone (PVP) as an agent when performing the impregnation-redox method. This allowed for more uniform dispersion of the platinum on the surface. The 5nm platinum particles were not coagulating into 40-60 nm clusters anymore as a result. This improved the performance of the IPMC and had a granular

damming effect to stop or reduce water leakage. The treated IPMCs displayed a sharper response with no delays and a rise in force output

The direct assembly method was introduced as a new approach to IPMC fabrication. The process consists of mechanically depositing an electrode layer via brush or spraying which provides more control over the electrode morphology and characteristics. The process is discussed in details in [45], Nafion dispersion is dissolved into isopropyl alcohol and glycerol to increase viscosity. High surface area conducting powders are then added and the whole mixture is sonicated and stirred for 1-4 hours to achieve good homogeneity and dispersion of the metallic particles. There are two proposed version of the application. The first suggests painting a layer of the electrode using a brush and place the membrane in the oven at 130°C for 15 minutes after each layer. The whole sample is hot pressed at the end at 210°C and 20 Mpa. The second version consists of painting all the layers on a Teflon reinforced glass fabric. The entire fabric is hot pressed on the sample using same temperature and pressure. After cooling, the sample is hydrated and the fabric is removed.

It's application in [19] showed larger capacitance and strain output compared to the impregnation/redox method.

Another advantage of the DAP is that it allows the usage of different conducting materials that were not feasible to be chemically reduced. In the case of [45] and [19], ruthenium dioxide was used as the conducting material. They did report that the surface conductivity was not enough and at the end additional platinum layers were added or electroplating a gold leaf. This is due to the fact that ruthenium dioxide displays good capacitance but high surface resistance going beyond 290 $\mu\Omega$/cm [53]. To solve or mitigate this issue, a solution of gold and ruthenium was tested [54]. Ruthenium has a high capacitance at low frequency but high resistivity at high frequencies. The addition of gold reduces slightly capacitance but also reduces resistivity. Reduction in resistance means a faster response but a reduction in capacitance also means a lower strain

DAP was applied in [55] in combination with ionic liquids in order to boost the performance of IPMC actuators and solve the hydration issue at the same time. It was found that the samples operated in air with approximately 30% reduction is strain after around 250 000 cycles. The large strains produced also lead to a faster deterioration and the main cause was found to be delamination of the gold leaf due to poor adhesion with the membrane. This issue was solved by using a poly-urethane polymer (PUU) which is known to have good adhesion properties with gold[56]. The resulting membranes using gold and PUU lasted much longer than previous samples reaching up to a million cycle.

A different method for applying the DAP was used in [57] where the electrodes were formed using Micro deposition. It gave more accuracy in the architecture of the electrode compared to manually dispersing the solution. There were however some drawbacks, mostly in the droplet formation that sometimes led to clogging. The process needs further study to optimize it completely but provides insight on the advantage of using a more precise dispersion techniques such as printing

2.4.Nafion Properties

2.4.1. Thermal Properties

Extruding Nafion filaments and 3D printing of the respective membranes will require proper   understanding of the thermal properties of Nafion precursor. Since more attention has been given to the activated Nafion films compared to the Nafion precursor form, an extensive search is performed to find the required properties.

[35] reports that the 3D printed membrane sustained higher temperatures (380°C) compared to the Nafion pellets (300°C). This indicate that the material was subject to

annealing and highlights the importance of the thermal history of the material. Extruding at temperatures above 260°C would lead to lower viscosity but might backfire during FDM extrusion where it will be more difficult to melt the material and might need higher temperatures.

[58] performs a study on PFSI compound similar to Nafion in terms of copolymers used but with different number of side chains. They linked thermal stability to the content of -SO2F side chains. These side chains are the first to decompose and a larger weight loss is observed for higher content of these side chains. Also, crystallinity is reported to decrease with increase in side chains

11 heating and cooling cycles between 50°C-250 were performed. A weight loss of 0.1% was achieved, indicating the possibility of extruding the same material multiple times. This however was not recommended for Nafion where it is mentioned that it should not be extruded more than once [31]

A rheological study to understand the thermal properties of precursor Nafion was conducted by [59] where interesting insights were uncovered about the behavior. The viscosity change and sheer thinning characteristics were observed and a modified carreau model was generated. In addition, Elastic and loss modulus were obtained indicating that 200°C is the starting melt temperature of Nafion with a tan γ =1 at this stage. The change of viscosity with temperature is also observed but at a fixed strain rate. To take this into account, the viscosity can be decomposed into a product that depends on temperature and one that depends on strain according to [60]:

$$\eta = H(T)\eta_{T0}(\dot{\gamma}) \qquad \textbf{(eq.1)}$$

Where H(T) is An Arrhenius model. There are different models that can be used, [60] mentions the following model:

$$H(T) = \exp\left(\alpha\left(\frac{1}{T} - \frac{1}{T_0}\right)\right) \quad \textbf{(eq.2)}$$

Degradation temperature was estimated to be at 330°C although significant weight reduction is observed only at 400°C onwards [59]. The young's modulus was computed in function of temperature and showed a value close to 3 Mpa at room temperature

Beyond the rheological behavior, some basic thermal properties such as thermal conductivity, specific heat coefficient and thermal expansion coefficient are not readily available but highly needed for simulation studies.

The thermal conductivity for Nafion 1100 precursor was found to be 0.289 (w/mk) in [34]

[61] obtained thermogravimetric analysis (TG) and differential scanning calorimetric (DSC) measurements for Nafion membranes in acid and sodium form. The degradation mechanism for acid form turned out to be different than that of sodium form. In addition, the temperatures at the corresponding endotherm peaks of the DSC graphs revealed the stage of transition to ionic clusters and the onset of crystalline melting.

[62] performed DSG and TGA analysis on different forms of PFSI and precursor PFSI synthesized in their lab. Applying the ratio method of [63] the specific heat measured for precursor was estimated from the graphs to be around 1.2 J/g.°C for an ion exchange capacity of 0.88 (meq/g). The Nafion precursor with EW =1100 is reported to have an ion exchange capacity of 0.98(meq/g) [34]. Its specific heat was approximated from the graph to be around 800 J/g.°C after interpolation with the specific heat corresponding to an 1.02 ion exchange capacity (meq/g) In the copolymerization stage, Polytetrafluoroethylene chain is estimated to have a size raging between 3-8 elements. Nafion precursor is reported to have a size of n=6.5. Also, they reported that the acid PFSI had the same structure as

Nafion 112. Therefore, the values obtained for the specific heat of the precursor were considered close enough for an initial approximation

The relationship between number of chains and EW is found according to the following equation [64]:

$$EW = 100 \times m + 446 \qquad \textbf{(eq.3)}$$

2.4.2. Chemical Treatment

Chemical activation of Nafion precursor starts by a hydrolysis step. A mixture of 15%Wt DMSO 35% Wt KOH and 50%Wt Deionized water is used to replace the SO2F side chains of the precursor [20]. DMSO is used to swell the membrane and the fluorine ion is replaced with the hydroxyl group OH-. The H is then replaced by the potassium ion K+ [65].

According to [65], the hydrolysis proceeds inwards from the surface. Once a layer is hydrolyzed, K+ and OH- ions can diffuse to the next layer and target the next SO2F group.

Based on experimental results, a rate of 1.3 µm/min was estimated when hydrolysis takes place at 75°C [65]. This rate can drop down with decrease in temperature, reaching durations of 48 hours for a temperature of 25°C

The change from precursor to ionic form was observed using SAXS patterns [65]. Continuous cluster formation was observed even after hydrolyzing the first layer indicating that it is a slow process and changes continue to take place even after the hydrolyzing front crosses the entire membrane.

2.5. Die Swell

Die swell is a complex rheological phenomenon that takes place during hot melt extrusion. When exiting the nozzle of an extruder or die, the produced filament part increases in size or swells to reach geometrical sizes larger than the die orifice extruded from.

Also termed the Barrus effect in some parts of literature, it is an attribute of the viscoelastic nature of the material and very common for polymers. Under the hood, the random polymer chains that are coiled in a random coil configuration are disentangled and rearrange based on the flow direction. After exiting the die, the material tries to get back to its original geometry, it has a shape memory due to its elastic properties.

When subjected to shearing, flow occurs when the molecules start sliding against each other. In that case the random coils are disentangled and rearranged in the flow direction. Therefore, as the shear rate increases, more chains will be rearranged in the flow direction and the viscosity will decreases. Simultaneously, the elastic energy will increase. Once the material exits the orifice of the extruder or die the molecules and chain will be subject to partial elastic recovery to get back to their original state [66]

Die swell occurs in two steps. At first, a sudden large change in diameter is observed followed by a slow increase across time in second stage [67]

From a practical perspective, guarding against die swell or being able to predict and control the percentage of swelling is of outmost importance for 3D printing applications. The filament tracks in FDM are 1.75 mm or 2.85 mm in diameter with very narrow tolerances. A filament with slightly larger dimensions would lead to clogging and disrupt the printing process. In addition, the extrusion process should achieve good uniformity in terms of diameter dimensions throughout the entire filament to avoid any clogging. Studies that have used single screw extruders and off the shelf filament making machines have used in conjunction a drawing mechanism to draw the filament from the extruder and wind it on a spool [20]. The RPM of both extruder and drawing motor are tweaked to achieve proper dimensions sizing. In this case, the drawing mechanism introduces elongation forces on the filament in conjunction to the shear forces exerted from extrusion, this changes the viscosity and the rheological response of the material [68]

To be able to successfully control, mitigate or even predict the percent of swelling, proper understanding of the different triggers and agents involved in the process is required. [69] reports that die swell is affected by the following factors:

- Shear rate/stress
- Polymer molecular weight distribution
- L/D ratio of the die
- Difference in diameters between reservoir and die

Mainly, colder melt temperature and higher shear rates are found to increase die swell [70]. It was also found that forcing an extrudate through a colder die increases swelling [69]

Note that these parameters have different effects depending on the polymer.

A rheological study was performed on a fluorsulfonated—PTFE copolymer in [69] gave insight on the viscoelastic behavior of perfluorosulfonated polymers, similar to Nafion. Die swell ratio was found to increase with increase in shear rate for all temperatures. Uncharacteristic of typical polymers, the die swell ratio appeared insensitive to temperatures at the lower range studied (190°C), then it increased with increasing temperature until reaching 250°C where it started decreasing. Note that they had a large melt endotherm starting from 130°C and ending at 255°C. they attributed this phenomenon to different modes of melting and processing, above 250°C the entire crystalline structure was eliminated by melting leading to viscous flow. The viscosity and shear stress decrease as temperature is increased leading to lower recoverable shear strain and thus reduced die swell. At lower temperatures there exists a certain degree of crystallinity as proved by their thermal analysis results. This crystallinity restricts viscous flow and promotes entropic recoil effects to enable elastic recovery. In that case, die swell is found to increase with increasing temperature.

It also interesting to look at the die swell phenomena for polymer composites for the extrusion of a Nafion ruthenium mix.

A study on HDPE mixture with titanium dioxide (TiO_2) revealed that the die swell ratio decreases nonlinearly with the increase of the titanium dioxide volume fraction [71]. In the case of [66], under same shear rate, the die swell for composite filled polymers were found to be lower compared to the pure polymer melt. They also found that the die swell ratio decreases linearly with increase in orifice diameter. However, the pure melt was more sensitive to the diameter change compared to the filled mixture [66]. The same result was found for the temperature variation. The die swell decreases linearly with increase in temperature with the pure melt being more sensitive to the change than polymer filled solutions. It was concluded that the addition of fillers reduced the die swell behavior

2.6.3D Printing

3D printing or additive manufacturing has attracted a lot of attention and formed the third industrial revolution. It comes with multiple advantages such as rapid prototyping and a near net finish with no waste as there is no material removal and sometimes no need for additional processing or treatment.

There are multiple 3D printing methods such as laser sintering and EBM, each better suited towards a specific application. The most common method in the market is FDM 3D printing. A thermoplastic filament is extruded from a liquefier and deposited on a head bed. The prototype is built layer by layer until achieving the required shape

The filament is fed using stepper motors, it is melted inside a liquefier with the solid part acting as piston to push it through the nozzle [72]. This indicates that the stiffness of the filament will play an important role in the printability of a given material [73].

FDM is a discontinuous process and parts formed are usually weaker in terms if strength than parts obtained from different processes such as injection molding [74]. Even at 100% filling, parts still display voids under SEM imaging [75]

The review [72] looks over the different issues and problem that can arise during FDM 3D printing. One of the most important issues is buckling of the filament. When being pushed through the nozzle, the filament is subject to back pressure and pressure drops due to the friction in the system and the geometry of the nozzle. The pressure applied to push the filament needs to exceed this back pressure in order for proper flow to be achieved. On the other hand, the filament has a threshold pressure due to it mechanical characteristics, exceeding this value would lead to buckling and twisting of the filament. The equation of back pressure is given by [72]:

$$P_{crit} = \frac{\pi^2 E d_f^2}{16 L_f^2} \qquad \textbf{(eq.4)}$$

E: Modulus of elasticity (Mpa) d_f: filament diameter L_f: distance between gears of stepper motor and entrance of liquefier

Due to the differences in filament diameter and entrance of liquefier, [76] proposed a correction factor of 1.1 to get the true buckling pressure.

The candidate filament used in 3D printing is in general required to have high viscosity at low temperature to avoid slipping and premature extrusion while shear thinning characteristics are favorable during extrusion to reduce the viscosity and thus the forces/power needed to push the filament [77]

Increasing the temperature would lead to a decrease in viscosity and a better flow out of the nozzle. However, temperatures above a certain threshold could also lead to degradation of the filament used [72].

FDM is known to be an anisotropic process with greater strength in the axial direction of line layer placed compared to the transverse direction. This was proven from the mechanical results on printed Nafion membranes in [78]

The effect of cooling rate and in fill density on inter layer adhesion were investigated in [74]. The strength of the part decreased with increasing cooling rate. When considering a constant cooling rate, the strength was found to increase with infill density until reaching 90% and started decreasing

High printing speed require an increase in temperature in order to decrease the viscosity of the material. On the other hand, a very slow printing favors warpage of parts as the printed layer cools down before the next layer is deposited [79]

The interlayer adhesion is formed in two steps: surface contact and inter-molecular diffusion across the wetted surface [80]. Thus the strength of the interlayer adhesion is determined by the spread of the wet surface and the rate of molecular diffusion [80,81]

Although some thermoplastics can be easily and readily printed, expanding towards new materials such as metals and biological compounds for medical devices requires adjustment of hardware and printing parameters.

To mix with a solid filler, the polymer is required to display shear thinning capabilities in order to make the flowing process possible. [82]

[75] found that increasing the temperature increase the dimensional errors in the products since the viscosity decreases, the material increases in fluidity and is more difficult to control when depositing

2.6.1. 3D Printing Issues

Buckling and slipping of filament can result in an unsuccessful print [83]. The issue usually occurs for flexible filament with small modulus of elasticity. Solution would be to increase the diameter of the filament used or to decrease the distance between the gear and the entrance of the liquefier. The latter could be done by first switching to direct drive extrusion on FDM 3D printers instead of Bowden extrusion. Also, some extruder heads are designed for flexible filaments with unusually short distance to liquefier such as the flexitruder used in [35]which had a distance of 6.5 cm.

The nozzle geometry has a large impact on the back pressure. It was found that the pressure drop decreases with increase of nozzle angle and increase of diameter [84]

[85] proposed a screw extruder head that can overcome such issues and can be applied on any feedstock

[85] define the ease of 3D printing as general metric that looks at:

- the ease of bed adhesion
- maximum printing speed that can be reached without buckling or failure
- how frequent print failures occur
- flexibility and ease of usage of the filament

Filament buckling is an important issue faced when dealing with flexible filaments. To solve this issue, [86] increases the diameter to 1.8-1.9 mm and reduced the distance between the liquefier and the gears of the motor.

This is related to the back pressure of the filament in the extruder of the 3D printer. Another commonly used method is to increase the nozzle diameter in order to reduce back pressure on the filament. Study in [86] used a 1mm nozzle in order to 3D print polyethylene

Anisotropy is a common issue faced with 3D printed parts. It is attributed in the weak interlayer bonding in a specific direction [85]

2.6.2. Bed Adhesion

Bed adhesion is crucial to obtaining good finishing and good results in FDM 3D printing. Commonly, the heat bed temperature should be below the melting temperature but war enough to allow slow cooling of the material. It should also be close to that of the extruder to reduce temperature gradients on the material.

Semicrystalline thermoplastics are usually easier to 3D print since they tend to melt above glass transition temperature and promote better bed adhesion, amorphous polymers on the other hand softens [86]

It is a common practice in the 3D printing industry to use sprays and tapes on the heat bed to promote better adhesion of the 3D printed part. In [87] they used a layer of polypropylene on the heat bed as it had good adhesive properties with the polyethylene filaments used. [35] used Kapton tape for better adhesion of the Nafion samples.

Adhesion can be also improved by adjusting 3D printing parameters. Lower initial layer speed help by allowing more time for the material to deposit and stick properly to the surface [86]. Larger nozzle diameter also leads to more material extruded and larger line width formed and leading to better adhesion [86]

Although high temperature of heat bed is required in some cases, too high of a temperature will lead to distortion of the material as the part will not cool down properly. On the other hand, a temperature that is too low will lead to rapid solidification and cause issues such as warping [88].

High nozzle temperature also promotes better adhesion on the bed plate and better adhesion between the deposited layer thus increasing the mechanical strength of the printed specimen [72]. Concretely, this adhesion between layers is reported to occur through sintering and viscous flow which is a temperature dependent process [73].

Reducing the time between layer deposition should help with the adhesion process by reducing the cooling time. However, this will mean increasing the printing speed and this could lead to buckling if the pressure applied exceeded the critical pressure.

2.7. Polymer Metal Composites

In this section, preparation methods of polymer metal composites are explored to find a suitable method for Ruthenium Dioxide-Nafion. Then, the behaviors and characteristics of 3D printing polymer/metal composites are investigated in order to appropriately define the dimensions and tune the 3D printing parameters for the successful fabrication of an IPMC electrodes.

2.7.1. Polymer Metal Mixing

The electrodes will be made using a Ruthenium Dioxide-Nafion inspired from the DAP process in [45]. However, to allow later extrusion via 3D printing, the precursor Nafion is used instead of the liquid Nafion dispersion that is already in activated form.

Mixing plays a critical role at high volume content of metal (55% and above) as reported in [89] where jamming of the extruder can become an issue. On the other hand, it can become increasingly more difficult to wind the extruded filament properly at volume contents higher than 40% with increase in brittleness [90]

As the Nafion precursor is in solid pellet form, an appropriate mixing method should be used to form the polymer/metal composite solution. Physical mixing is a trivial option, the powder and Nafion can be placed in a mixing bowl at high enough temperature for the Nafion precursor to melt, in excess of 200°C [59].

Typical method for mixing and production of filaments involve the usage of screw extruders. A single screw extruder is good at producing homogenous filaments [91]. The shear generated by contact between the polymer, the screw and the barrel create enough force to cause the polymer to flow. They are not however very good in mixing different materials together into a homogenous solution with reported chances of agglomeration [85]. This particularly evident for polymers with very high viscosity [92]. The double screw extruder is better suited for mixing problems as the added friction between the screws helps generate more shear and better mixing [93].

The authors in [94] tried manually mixing the solution before placing it in the twin extruder. [95] used a plunger design where the metal powders are fed by a feedstock to the start of the nozzle and the piston pushed the thermoplastic out of the nozzle, mixing them together. Unsurprisingly, since the mixing does not happen before extrusion, the homogeneity and extrudability improved in subsequent extrusion trials of the same material, however the filament cannot be cycled indefinitely as it will be subject to degradation.

In terms of mixture quality, non-spherical fillers were found to produce low flowability due to mechanical interlocking. This interlocking is a function of particle size and shape [96].In addition, maintaining good homogeneity of highly concentrated mixture is critical as particles are prone to aggregate [97]. This also lead to mechanical interlocking and poor flowability.

A different approach found in literature is the usage of solution mixing before extrusion. The thermoplastic is dissolved in an appropriate solution and mixed with the metal powder. Once properly mixed, the solution is dried out to obtain a solid mixture that can be extruded. [86] tried this approach by dissolving ABS into acetone and produce good results in terms of homogeneity of mixing as revealed by SEM imaging. Similarly, [89] proposed a solvent mixing method where the thermoplastic where PLA was dissolved in a solution of dichloromethane and the nickel-copper powder was added gradually. The solution was dried out using a vacuum furnace and naturally dried afterwards to obtain a solid sample. It had lower viscosity in mixing and was able to accommodate a higher metal content before failure (62% vol compared to only 54% vol for physical mixing) [89]. However, it proved to have the same homogeneity of the result compared to a physically prepared mixture at 50% vol. This method proves to be easier to use if an appropriate solvent is found, however this is not available for a combination of Nafion and Ruthenium Dioxide. Given the optimal loading of Ruthenium Dioxide in Nafion is around 42% vol [45], physical mixing can still be used for this case.

The mixing rate or the speed of the extruder is critical for a good mixture. An increase of speed would lead to high temperatures but also high shear rates. This accelerates polymer degradation similar to the results observed in [87].

Good mixing is a key factor for any polymer metal composite application, [98] reported a loss of performance of the polymer metal composite due to poor adhesion and lack of homogeneity between metal particles inside polymer matrix

2.7.2. Polymer-Metal 3D Printing

3D printing polymer metal composites is a less trivial task compared to regular 3D printing of thermoplastic filaments. [99] reported high surface roughness for metal 3D printed parts while significant porosity was also noticeable between the metallic particles and polymer matrix [100]. This was linked to the extrusion process and can be mitigated by increasing the metal content to a certain extent [101]

2.7.3. Characteristics Polymer Metal Mix

According to [89], the addition of metal particles would obstruct the disentanglement and rearrangement of the polymer coils. This would indicate more difficulty in flowing but also reduction in die swell which was also confirmed in a previous section.

[102] used TiO2 as an additive to ABS polymer. The result was a more brittle surface compared to the previous filler free case.

[94] found that as solid loading increased above 15 % wt, the ultimate tensile strength of ABS- stainless steel mixture reduced. It was theorized that the increased loading leads to more increased stress concentration between polymer matrix and metal particles and leads to easier formation of fractures. Higher loading also shown to ease the propagation of fracture. They highlighted an important issue in polymer-metal composites which is the lack of interfacial adherence between metal and polymer particles. The irregular shape of the powder for their case led to interlocking with the polymer matrix but SEM images showed incomplete adhesion.

The results in mechanical properties vary in studies depending on the proper adhesion and mixing between polymer and metal particles. The results in [85] showed an increase in maximum flexural strength and modulus of elasticity for a polyethylene-copper while this was not the case for studies in [94]

Multiple studies such as [86,94] report however an increase and later on a decrease in mechanical properties with an increase in metal loading. SEM imaging in [86] showed the empty cites in the polymer matrix increased with increase in copper loading which would ultimately lead in a decrease of tensile strength. Similar results were found in [103] -where an increase in copper loading led to a decrease in tensile strength of ABS and an increase in the percentage of voids present. The authors theorized that the increase presence of copper in the polymer matrix disrupts the bonding forces and leads to a reduction in tensile strength. However, [103] also reported an increase in thermal conductivity and a decrease in thermal expansion coefficient with increase in copper loading, resulting in less distortion issues with the 3D printed parts

2.8.Filament Making

Most common method is the use of a filament extruder which can be designed such as [104]. [37] used this approach to produce their filaments, they had to do multiple trial and error runs to dial in the required rpm for both extruder and drawing mechanism.

Some studies such as [94] use of the market filament extruders. They face the same issue of having to tweak the rpm and use a drawing mechanism. Although depending on the device purchases, its capabilities might be limited in contrast to building an extruder tailored for high temperature and high viscosity applications such as the extrusion of Nafion.

[86] uses cooling bath before reaching the drawing mechanism. [85] use single/ twin extruders to produce the filaments.

Extrusion part play a key role as it affects the orientation of the particles [105] and leads to anisotropy in terms of mechanical and electrical properties [106]

CHAPTER THREE

METHODOLOGY

3.1. Instrumentation and thermal sensors

Temperature control is crucial in multiple areas of the project. Accurate and precise temperature control is needed for the extrusion process. In addition, monitoring of temperature variations in DAP mixing, chemical procedures and 3D printing process is needed

For choice of sensors, a PT100 RTD taken from the extruder head of the ultimaker 3 was used and calibrated. Look up tables from the manufacturers were used and the data of resistance variation vs temperature was curve fitted via Matlab for a range of 0-400 °C.

Figure 2-Curve fitting of PT100 data

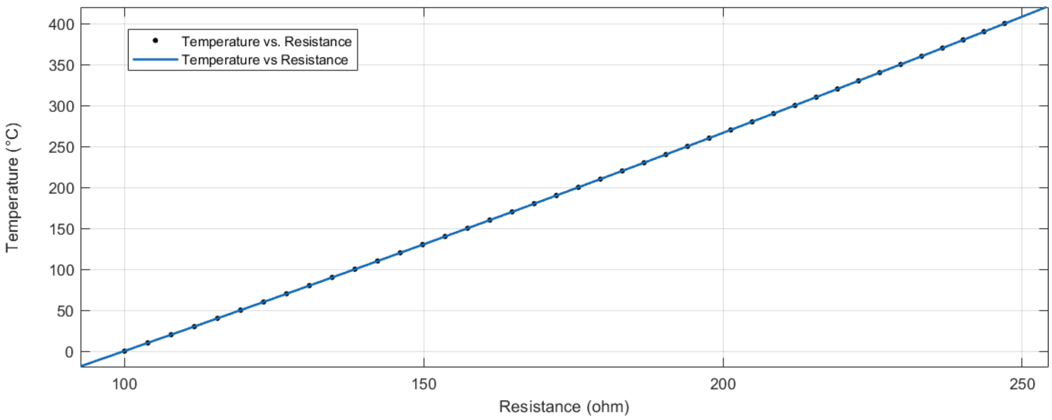

Taking into account nonlinearities arising from RTDs, a second order polynomial was fitted to the data. It resulted in an R^2 of 1 and the following equation:

$$T = 0.001161R^2 + 2.315R - 242.9 \qquad \textbf{(eq.5)}$$

To detect a temperature change, the PT100 sensor is connected to a Wheatstone bridge. A 100 ohm-1000 ohm branch arrangement was chosen, this is needed in order to reduce the current. High currents lead to sensor self-heating and erroneous results. The circuit is shown in figure.3 Below:

Figure 3-Wheatstone bridge arrangement

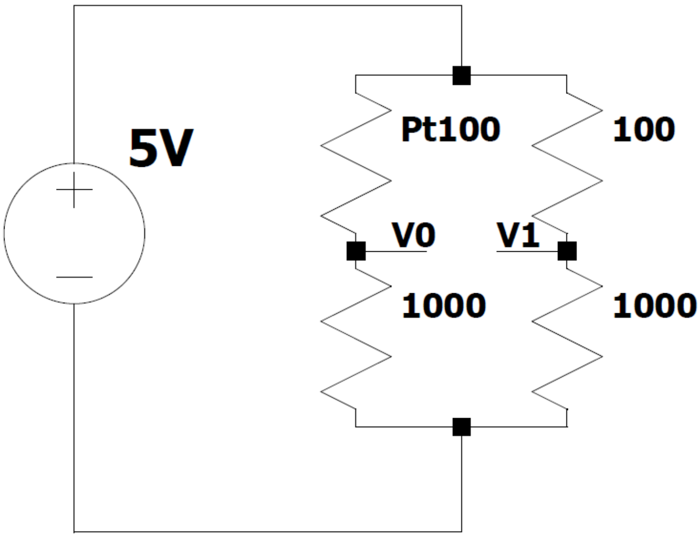

The 5 Volt difference was provided by an Arduino Uno. The Pt100 has a resistance of 100 ohms at 0 °C, the Wheatstone bridge would be balanced in that case.

When the bridge is unbalanced, the resistance of the Pt100 sensor can be determined by measuring the differential voltage between the two branches:

$$V = V1 - V0 = 5\left(\frac{R_{Pt100}}{R_{Pt100}+1000} - \frac{100}{100+1000}\right) \quad \textbf{(eq.6)}$$

Rearranging gives:

$$R_{Pt100} = \frac{1000\times A}{1-A} \quad where\ A = \frac{V}{5} + \frac{100}{100+1000} \quad \textbf{(eq.7)}$$

The sensitivity of the sensor is given by the slope of the calibration curve [107]:

$$S = \frac{dT}{dR} = 2.315 + 0.0023R \quad \textbf{(eq.8)}$$

The variation of resistance vs temperature can be also obtained given by:

$R = (-5.777E - 5)T^2 + 0.3908\, T + 100$ **(eq.9)**

Sensitivity is given by:

$S2 = \frac{dR}{dT} = 0.3908 - (1.1554E - 04)T$ **(eq.10)**

Almost a 0.4 ohm/°C change.

A second choice of sensors was the NTC 3950 100k used in the ender 3 heat beds. This thermistor has a temperature range between 0-300°C. Look up tables were available as well leading to the following power law relationship when curve fitting using Matlab

To validate the quality of the product from the manufacturer, the NTC sensors were calibrated with respect to the PT100 RTD. Both sensors were attached to the surface of the ender 3 heat bed for this experiment. The heat bed temperature was raised 5 °C in successive interval and the values were recorded via Arduino which was interfaced directly on Matlab. Since the surface temperature was measured, both sensors were covered with fiber glass to minimize convection from the ambient environment.

3.2. Flow of Nafion precursor

For a successful filament extrusion and printing process, a good understanding of the flow behavior of Nafion precursor is required.

The thermal properties found in literature are used to set up a model using Ansys PolyFlow in order to capture the die swell behavior

Modeling die swell is a complex phenomenon. One has to rely on constitutive equations to represent the flow behavior. There are integral based methods and differential viscoelastic equations used in literature. For this study, the Giesekus model was used to model the flow of Nafion precursor. From the different differential viscoelastic model, it has only one hyperparameter to tune, the mobility factor “α”, and provides good representation of the die swell effect.

Giesekus model equation is given by:

$$\tau + \lambda_1 \frac{d\tau}{dt} + \frac{\alpha}{G}(\tau.\tau) = 2\eta_0 d \qquad \textbf{(eq. 11)}$$

$$G = \frac{\eta_0}{\lambda_1}$$

The viscosity in function of strain rate is given by:

$$\eta(\dot{\gamma}) = \frac{\eta_0(1-g)^2}{1+(1-2\alpha)g} \qquad \textbf{(eq.12)}$$

Where g is given by:

$$g = \frac{1-f}{1+(1-2\alpha)f} \qquad \textbf{(eq.13)}$$

And f:

$$f^2 = \frac{\sqrt{1+16\alpha(1-\alpha)\lambda_1^2\dot{\gamma}^2} - 1}{8\alpha(1-\alpha)\lambda_1^2\dot{\gamma}^2} \qquad \textbf{(eq.14)}$$

The coupling of the equations is highly non-linear. To identify "α", a numerical optimization method is used. The viscosity in function of shear rate is provided already by [59] in the form of a modified fitted carreau model

Genetic algorithm is used to solve equation by minimizing the following fitness function:

$$fit = (\eta_{giesekus} - \eta_{modified\ carreau})^2 \qquad \textbf{(eq.15)}$$

Which is minimizing the squared error between the viscosity obtained from the modified carreau model and the viscosity obtained from the Giesekus model.

Once "α" is obtained, all values are plugged into Polyflow to approximate the die swell ratio of an extruded Nafion filament

3.3. Membrane preparation

In the course of this study, the Nafion membranes used will be prepared by 3D printing and hot pressing.

3.3.1. Hot pressed membranes

The hot-pressing samples are used as validation to investigate the polymer metal mix without being affected by the 3D printing process. The procedure adopted is inspired from the work in [21]. Two aluminum plates were used and covered with Kapton tape to avoid the issue of sticking. However, since the Nafion is in pellet form, high temperatures were used to melt the pellets into a uniform membrane. In addition, the hot press used did not have any possible way to accurately control the pressure. The only way to do that was to increase the spring tension by decreasing the distance between the sample and the heated plate. Multiple trial and error attempts were needed to obtain membranes with a small thickness and homogenous texture.

The process was repeated until getting a uniform texture for the membranes. Early removal of membrane resulted in visible boundaries marking the location of the pellets and indicating that the pellets are not homogeneously fused together.

In addition, one sample will consist of a Nafion membrane sandwiched between two membranes of Ruthenium Dioxide-Nafion mix with the same volumetric loading of 42%. For the Nafion membranes, samples were left at a temperature of 220°C for a duration ranging between 5-8 min.

When heat pressing the Ruthenium Dioxide-Nafion mixture, more pressure was required due to the increased stiffness and the process was performed at 230°C instead. Two membranes made of polymer metal mix were obtained with a thickness of 0.1mm. Their dimensions were slightly increased to make the assembly process with the Nafion membrane slightly easier.

3.3.2. 3D printer set up

Since both electrodes and membranes were going to be 3D printed, the device used should be optimized for both conditions. This section summarizes the analysis adopted and steps taken to customize the 3D printing machine.

The 3D printer used in [14,20] was a Mendel 3D printer custom made. The key operating points were:

- Direct drive extrusion
- Heat bed of 180°C
- Extrusion temperature of 275°C

These specifications are challenging to find on common commercial FDMs. Bowden extrusion is the most common extrusion method found, however it is not suited for flexible filaments such as Nafion. Hotends reach extrusion temperatures of 200°C in most cases. The heat bed is also limited to 110°C to protect the PCB board.

In addition, 3D printing the electrodes would require a polymer/metal blend filament to be extruded. This would damage the copper nozzle typically found in the extrusion head and lead to inaccurate dimensions and irregular flows

Instead of assembling a custom 3D printer from scratch, the Creality Ender 3 model was chosen. In addition to being affordable and reliable, it is also open source in terms of Firmware and has not shortage of custom parts available on the market.

To solve the extrusion issue, an all-Metal extrusion kit provided by Microswiss was used to upgrade the extrusion head. The heat sink is made of titanium alloy, allowing better heat dissipation. This permits 3D printing at higher temperatures without damaging the hotend. An aluminum framing is used to switch from Bowden extrusion to direct extrusion, it also provided good thermal dissipation, protecting the DC motor.

The path of the filament if constrained by the PTFE tube with the chamfer ending reaching the driving gears.

The stainless-steel nozzle is also provided to protect against wear and abrasion. Additional stainless-steel nozzles were brought in as well.

The same DC motor is used for the extrusion part. it is now mounted on the aluminum frame of the hotend instead of the printer chassis frame. This means that there is increased inertia on the x-axis of the machine. As a result, printing speeds should be reduced in order to avoid excess jerking and vibrations. The small pushing gear mounted on the DC motor arm is replaced with a finer version provided by Microswiss, which is better at pushing flexible filaments.

The original temperature sensor and heater cartridge provided in the ender 3 model can still be used. The temperature sensor is an NTC 3950 100K thermistor and can function well up to 290-300°C

For the heater bed, the original one is a PCB board running on 24V 220W and can withstand up to 110°C. A silicon heater pad was bought and attached to the original PCB. The NTC 3950 100k thermistor taped under the PCB is removed. The new silicon heater pad, rated at 500W 220V AC, is attached instead. The pad had an imbedded temperature sensor of same specifications. This will allow the printer bed to reach and maintain 180°C without any damage and in a shorter amount of time, given that there is not heating chamber used for the current device.

Given that the new heater pad operates on 220V AC voltage, it cannot be connected directly to the ender 3 main board. The board itself is powered using a 24V 15 A power supply connected to 220VAC. A 0-32VDC/24-380VAC solid state relay, rated at 15A, is used to control the heater pad. The controlling DC port of the SSR are connected to the ports on the ender 3 board previously used to power the original heater bed. The heater pad is then connected, through the SSR, to the main AC power supply. The printer can now control the heater pad via the SSR, which provides a very fast response time. This is crucial to obtain good print quality. Although the expected current consumption is approximately 2.3 A, a higher rated SSR would have better heat dissipation and operate for a longer time.

However, going above 110°C means the adhesive build surface originally placed on the PCB will deteriorate. It is removed and replaced by a 4mm tempered glass surface better suited for high temperature printing. It also provides better surface finish when dealing with complex materials

After fitting the new components, calibration procedures followed to ensure all components were working as they should.

The firmware was updated from the old Creality ender 3 firmware to the newest version of TH3D. Both firmwares are based on the Marlin firmware code. However, TH3D comes with some additional functionalities and features such as thermal runaway protection. The code is written in C++ language and the main code header file can be easily opened from any coding environment such as Visual Studio code. From there, thermal runaway is uncommented. The maximum temperature of the hotend is allowed to reach was changed to 285°C. The maximum temperature of the heat bed is increased to 185°C, leaving room for possible temperature fluctuations. Finally, the PID calibration mode was enabled instead of the original Bang Bang method. This allows faster response and better control. This is crucial in order to not damage the filament from overheating during the extrusion and ensuring good quality of the printed part. The range temperatures were allowed to vary was reduced from ±10°C to ±3°C.

PID auto-calibration is performed for both heater bed and extruder. The printer is connected to a laptop via the Octoprint software. This program enables us to monitor the

3D printer parameters throughout the printing process and execute G-code commands via a command window.

For the extruder the PID auto tune is done using the following steps:

- Enter command: M303 E0 S280 C10. E0 designates the extruder. S280 indicates tuning for a target temperature of 280°C. It is better to calibrate for the temperature required during the operation. C10 indicates the auto-tuning process will repeat for 10 cycles.
- The command window will display the values for the proportional, integral and derivative parts of the PID. The command - M301 P20.22 I1.22 D84.07 is used to save the values in the printer software in the respective order mentioned.
- M500 will save the values in the EEPROM of the machine to be used in later prints.
- M503 to verify by generating a report of the current settings used during printing

For the heater bed, the same process is applied with the following parameter changes:

- M303 E-1 S180 C10. E-1 indicates the heater bed and the target temperature is 180°C.
- M304 P212.85 I33.74 D895.11 instead of M301 command.

The extrusion calibration consists of two parts. First the E-steps calibration is performed. This adjusted the amount of filament extruded in millimeters per DC motor step. The new components installed this would have different friction forces and would require a different ratio. The procedure goes as follows:

- The filament used is marked with a 20cm distance measured
- An extrusion of 10cm is indicated on the printer
- The actual extruded distance is determined by measuring how much of the 20cm label distance was extruded.

- Using command M503 to generate the printer settings, the current E-steps value used is located on line M92.
- The actual E-steps value is computed as follows:

$$Esteps_{current} = \frac{Number\ of\ steps\ (steps)}{Length\ extruded\ (mm)} \qquad \textbf{(eq.16)}$$

This can be re-arranged to:

$$Esteps_{current} \times length\ chosen\ (mm) = Number\ of\ steps\ taken$$

The actual extruded length by the machine is computed by:

$$Actual\ Extruded\ length = Measured\ length_{start} - Measured\ length_{end}$$

The actual E-steps are found as:

$$Esteps_{actual} = \frac{Number\ of\ steps\ taken\ (steps)}{Actual\ extruded\ length\ (mm)} \qquad \textbf{(eq.17)}$$

- The obtained value by using the command M92 ###.# and replacing the #’s with the obtained digits.

The next part consists of calibrating the flow rate. This part is based more on trial and error approximations.

- A test file of known dimensions is loaded into the slicing software. Cura 4.1.1 was used in the current process.
- The print settings are adjusted. Flow rate is indicated to be 100%.
- The printed part is measured. Based on the dimensions offset, the flow rate is either increased or decreased.

This step is repeated multiple time to get the right dimensions. The flow rate can be adjusted at the first layer and increased slightly to promote better adhesion.

One should note that this process does not apply to flow rate only. Multiple test files can be found, each used to stress or determine the quality of the printed part from different aspects: flow rate, structure integrity etc.

3.3.3. 3D printing process

A simple 15mm x 5mm x 0.5mm design for a Nafion membrane was prepared as an STL file and loaded in Cura. Settings were tweaked based on trial and errors to achieve the following criteria:

- Strong bed adhesion
- Good and constant flow of Nafion
- Good geometrical integrity of the part

The bed temperature was raised to 185°C as recommended in for good bed temperature. The set up however struggled to reach 185°C on the glass heat plate. The outer, unused areas of the plate had to be covered with fiber glass insulation in order to reach the require temperature. This was confirmed by multiple heat tests with NTC 3950 100k sensors attached on multiple locations of the glass plate.

To obtain good flow of Nafion, a multiplier factor of 1.5-1.6 was used on the flow rate given that the calibration is done on PLA material. The printing speed was also reduced to 1 mm/s in order to avoid buckling of the filament. Given that the diameter achieved was 1.6 mm, there were still issues of buckling and jamming when printing at higher speeds. Note that in this case a stainless steel, 0.4 diameter nozzle was being used.

3.3.4. Filament Fabrication methods

In order to be 3D printed, the Nafion pellets have to be reformed into a filament 1.75 mm in diameter. Close tolerances are required to avoid any clogging in the extruder head of the ender 3. The Capricorn tubing has a diameter of 1.95 mm ± 0.05 mm which should not be exceeded.

Two methods were considered for fabrication of the filaments: extrusion and injection molding. Initial prototypes of the latter showed that it will require a large pressure to avoid the formation of voids in the filament [109]. Single extruders can be used or piston cylinder assemblies to provide the required flow and pressure. In addition, pressure should be applied to the mold via a clamp mechanism to keep the two halves as tight as possible and be able to remove them afterwards. Another point is proper venting [109], openings for the gas to escape should be considered in the mold design. These vents would fill up with material and produce waste that is very expensive for the case of Nafion. For all the above-mentioned reasons, building an injection molding device from scratch was not cost efficient.

There are multiple designs of extrusion mechanism in literature, most based on the single screw extrusion mechanism, especially in filament fabrication [110]. The concept would require feeding the pellet via a hopper into heated barrel containing a single screw. Therefore, the screw design is essential as the diameter will vary throughout the regions. A stepper motor is used to provide the required speed for small application and the polymers or plastic exits the barrel via a nozzle. For polymers and viscoelastic materials, the phenomena of die swell is observed during extrusion [110,111] in most cases. Upon exiting, the filament diameter increases in size, this could make the filament not suitable for 3D printing in case the swelling is too large. To solve this issue, a spool is used to draw the exiting filament. The spool exerts and extension force on the filament leading to diameter shrinkage. This has been used with both DIY extruder and filament making devices available on the market. The polymer filament is subjected to shear and extensional flow characteristics, referred to as mix flow [112], this will be discussed further in later sections. It is a trial-and-error concept where the spool turning speed and the extruder speed are varied until the required filament diameter is achieved. This is also an expensive process in Nafion, since it is not recommended to reheat Nafion filaments more than once.

Instead, a traditional plunger-based extruder mechanism is used, similar to the one in [79]. The set up consists of a vertical assembly 35 cm high with an aluminum block bolted on it. The plunger, shown in Fig.1, is welded on the aluminum block. It has a 2.55 cm outer diameter and 8 mm inner diameter, made out of aluminum alloy A4043. The plunger is 14cm long with the upper part (7cm) threaded with a 2mm pitch thread. The device was made vertical to take advantage of gravitational forces. They can produce an extension stress that acts similarly to a drawing spool. The filament in this case, would be limited to approximately a maximum of 30 cm and thus restricting the sizes of the shapes that can be manufactured with it via 3D printing.

Figure 4-Extrusion system

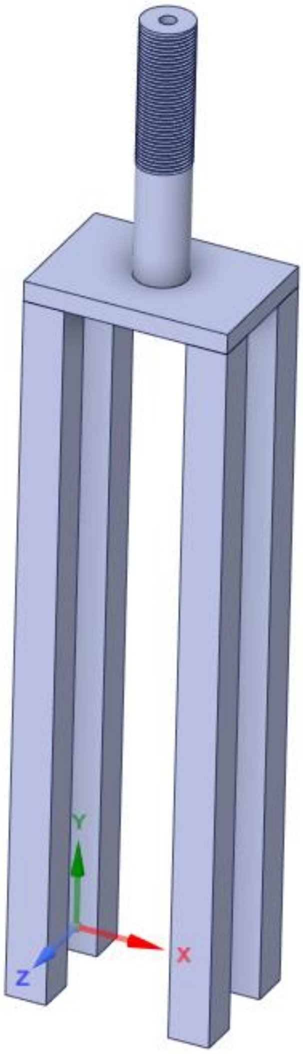

A small nozzle of length 5.76 mm and 1.6mm in diameter is drilled at the end of the plunger head. This led to a very low L/D ratio which is not recommended for extrusion application, it is limited to the manufacturing capabilities available as longer drill bits of size 1.6mm are not available.

To avoid any material slippage, the piston is 8mm in diameter with close tolerances. It is made of stainless steel connected to a hollow cylinder. The cylinder is threaded on the inside with a 0.8 cm diameter and an outer diameter of 2.55 cm. A handle is welded on it to make it easier for handling. The piston moves 2mm/turn and the handle makes it easier to apply large torques. However, the speed will be inconsistent since it is operated manually and has a risk of leading to fluctuations in diameter. This issue can be addressed by connecting the piston head to a stepper motor in the form of a linear actuator in future designs.

Figure 5-Plunger head design

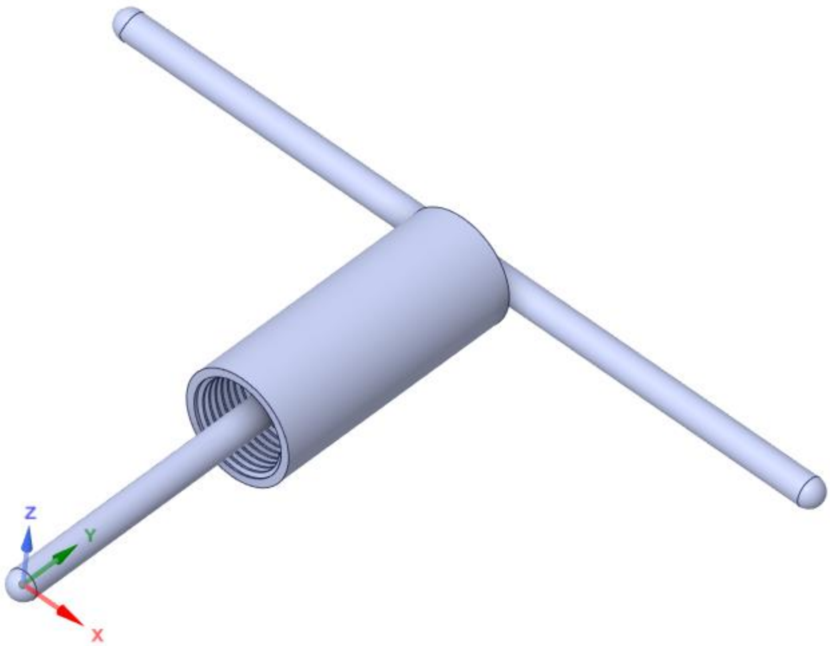

The head was smoothed out to make it as conical as possible, the same was applied to the bottom of the plunger just before the nozzle. This design is used to avoid sudden elbows and changes in diameter and decrease the shear strain. Unfortunately, the length of the conical area was limited to the manufacturing capabilities available.

Rheological experiments showed that Nafion starts melting at 200°C [59]. A previous study that focused on 3D printing Nafion found the ideal temperature for Nafion extrusion to be 285°C [14]. This could be linked to the combination of decrease in viscosity due to increase in temperature combined with the extrusion speed and drawing speed used. For the current large set up, it would be challenging to reach this temperature by heating the bottom part of the plunger alone. A two-fold heating strategy is proposed, the setup is placed in a thermal mold (Fig.5) containing 4 electrical heating elements, with a combined power of 400W supplied from a 220V AC source. The thermal mold is built out of thermal clay bricks and thermal clay with holes drilled for electrical wiring. Insulated wires were used for electrical connections. A second heating source is provided by wrapping a nichrome wire around the bottom part of the plunger. This will provide direct heat to the pellets inside the plunger while the electrical heating elements would be used to heat the structure and provide and ideal temperature for slow cooling of the filaments.

Figure 6-Thermal Mold

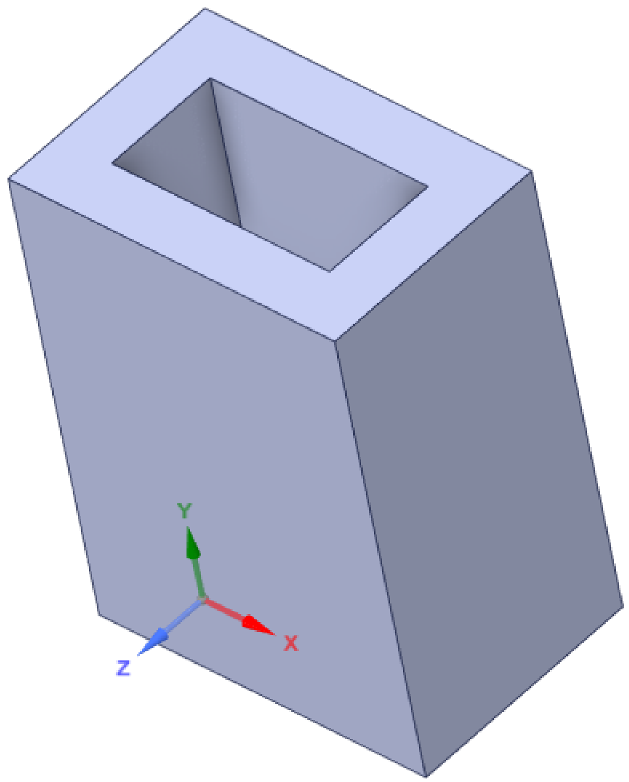

The thermal mold is made of bricks of size 20cm x 10cm x 5 cm. it has a 40 cm height, 20 cm width and 10 cm depth. The bricks were assembled using thermal clay as well. It is estimated to handle temperatures of 1000°C. However, it is not made of refractory material, as such it is subject to heat loss on the sides by convection and has a high specific heat as initial heating test have shown. Fiber glass insulation was used by wrapping two rolls around it and using smaller pieces on top to limit heat loss as much as possible. Limiting heat loss not only increases the temperature that can be reach but also improves the ability of the mold to maintain a high ambient temperature for a longer time.

Before welding the plunger head to the extrusion stand, heating experiments were conducted to investigate the heating capabilities using nichrome wires. The bottom part of the plunger head was wrapped using a nichrome wire with 10 turns at first. Kapton tape is wrapped around the heated part before placing the wires and after placing them to avoid contact with the aluminum body and any short circuit. Nichrome is reported to have a low conductivity of 0.13 w/m.k[2] but can support temperatures of up to 400°C without degrading. Three NTC 3950 100k thermistors were placed across the plunger head:

- At the bottom near the nozzle
- In the middle between heated and not heated regions
- At the top

Results after one hour of testing using a Voltage of 25.3 V and current of 0.81 amperes. The results are shown in fig.4. it is clear that there is relatively good heat conductivity as the temperatures of all sensors were very close to each other. However, the max temperature stagnates at around 198°C after one hour. Given that this test was applied on the plunger head only without the rest of the set up clearly indicates more than one heating source is needed.

In order to get the maximum heating power, the following equations has to be maximized:

$$P_{heating} = R \times I^2 \qquad \textbf{(eq.18)}$$

Since it is proportional to the square of the current, increasing the current would provide more power than increasing the resistance. On the contrary, this would require decreasing the resistance. One also has to consider the limitation of the power supply used, a direct current power supply is used with a maximum voltage of 30V and a maximum current of 3A.

A four-wire kelvin test was performed on strips of nichrome wire of 0.2 diameter to determine the resistance of the wire per unit length and validate the suppliers' specifications along the way. Three strips were used of lengths: 16cm, 13.5cm and 9.5 cm.

By varying the voltage supplied, the resistance and subsequently the resistance per unit length can be calculated using equations 2 and 3:

$$R = \frac{V}{I} \quad \textbf{(eq.19)}$$

$$R_m = \frac{R}{Length\ of\ wire} \quad \textbf{(eq.20)}$$

This test gives more accuracy than using a two probe ohmmeter, the layout configuration is shown in fig.4 and the results are displayed in table.1:

Table 1-Results of 4 wire kelvin test

Wire length (cm)	Average Resistance per unit length (Ω/m)	Standard deviation
16	33.82823	0.071189
13.5	34.1979	0.219317
9.5	32.91045	0.326854

Resting phases were included between each measurement to allow the strip to cool down and avoid any issues of self-heating and change in resistivity. The supplier notes a 34.7 Ω/m resistance per unit length for a 0.2 mm diameter wire which is very close to the values obtained. A value of 34 Ω/m is chosen for the remainder of the calculations

Figure 7- 4-wire kelvin test configuration

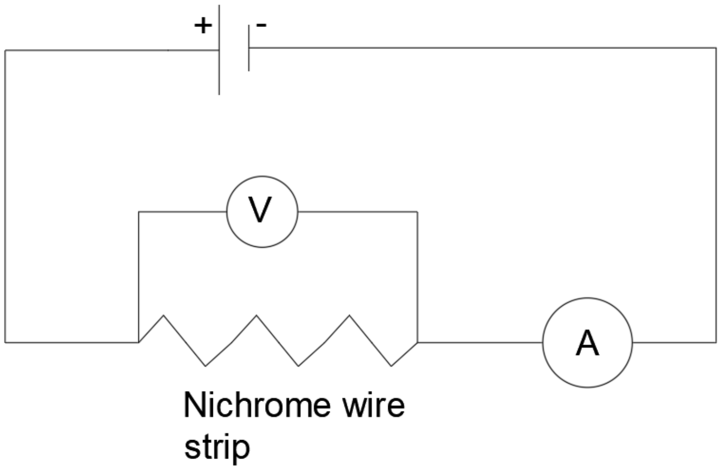

Upon running further heating tests using different number of turns, one notices that the nichrome wire heats up and starts glowing on few occasions such as for 4 turns with 23V and 1.5A. The power provided can be calculated also as:

$$P = V \times I \qquad \textbf{(eq.21)}$$

It seems that for a power close to 35 watts, the nichrome wire reaches close to 700°C (onset temperature for glowing). This can lead to localized Kapton tape degradation and short circuit.

The problem statement can be rewritten as maximizing equation.21, subject to the following constraints:

- Max voltage of 30V
- Max current of 3A
- Max power of 35 w

A Matlab code was used to go over different number of coil turns, a total of 8 turns gave the maximum power desired given the abovementioned constraints

The extrusion set up is placed inside the thermal mold. Two 3950 100k NTC thermistors are placed at the bottom of the plunger head and top of the plunger to monitor changes in temperature. An additional sensor is wrapped in an insulation sheet and covered in thermal insulating silicon before being placed hanging inside the thermal mold to cover the ambient temperature.

The nichrome wires wrapped on the plunger head are connected to the DC power supply and controlled via an electro-mechanical relay rated at 5V and 10A. The electrical heaters are connected via solid state relay rated at 15A. An Arduino uno is used to toggle the relays and read the sensor data. In order to avoid local hotspots, especially if the structure falls very close to the heating elements, the heating strategy consists of heating for 40 seconds with 5 resting seconds afterwards. The whole process takes around one hour for the ambient mold temperature and plunger temperature to reach 240°C which is the maximum temperature targeted.

There is a possibility of witnessing HF gas emissions while heating, this was mentioned in [59] and [36]. [36] reports traces of HF gases, notably in situations where Nafion degradation starts but advocates for the usage of (other material) to avoid part erosion. A fume hood was used in [14], this is not practical for the current set employed. The alternative proposed here is heating the Nafion elements at a temperature of 110°C for a period of 30 min to 1 hour. This temperature guarantees that the Nafion is far from melting and, given that HF gases for by reaction of water molecules with any fluoro based polymer, the procedure would lead to moisture removal from the material before starting the melting procedure.

Nafion is reported to start melting at around 200°C according to [59] where the loss modulus became higher than the storage modulus. As temperature increases the viscosity will decrease making the extrusion process easier. The change in viscosity in function of temperature was reported in [59] for a strain rate of 1 rad/s. the data was fitted using Matlab to obtain an equation of the approximate Arrhenius law:

H(T)=-0.02423(T-220) **(eq.22)**

Low viscosity is required when extruding but rapid solidification is preferred afterwards to preserve the shape of the filament when exiting. In addition, polymers are subject to annealing when extruded at high temperatures eg. if a Nafion filament is extruded at 210°C, it will take heating up to 210°C to melt it again. This could cause problems for the 3D printing phase with the customized ender 3 limited to 300°C. Therefore, the temperature was limited to 240°C.

Initial extrusions were done at 220°C.,230°C. and 240°C. The target was not to exceed 1 mm displacement inside the nozzle to allow time for the material to relax inside before extrusion. Also, very low speed and strains were favorable to keep the material in the Newtonian phase or at least linear viscoelastic regions. The viscosity curve in [59] showed a small plateau at strain rates below 0.1 rad/s (to be checked). The results were filaments of diameter smaller than 1.7 mm that broke easily while extruding, leading to multiple small filaments. It is speculated that the filament thinning is due to excessive extension stress from gravity. As the filament drops down, the hanging mass increases and thus increasing the force applied. This led to localized very thin diameter that could not handle the weight of the filament and subsequently broke. To counter act the problem, a moving platform was bolted on the aluminum block. The platform would have a varying distance with respect to the nozzle. This would allow us to collect the filament at smaller distances and decrease the effect of gravity. Also, the extrusion speed was increased to induce more die swell. This resulted in thicker filament but there was still an issue of excessive thinning and filament breaking. The best result obtained was a 20 cm , 1.2 mm in diameter filament. It was obtained at high speed extrusion of temperature of 240°C for mold and plunger and 7 cm distance from the nozzle.

An alternative was to employ solid state extrusion. This procedure extrudes polymers below the melting temperature but above the glass transition temperature. This method is not only reported to prevent die swell, it also improves the mechanical properties in the extrusion orientation. This provides a huge boost as Nafion has low modulus of elasticity and was mentioned to be hard to print. A successful SSE would lead to a smooth filament and should be done below melting temperatures.

3.3.5. Chemical activation of 3D printed samples

The electrodes were made of a precursor Nafion mix with Ruthenium Dioxide. Therefore, the entire membrane should be functionalized and transformed to acid form.

The Ruthenium Dioxide electrodes presented very bad surface resistance and poor conductivity. To adjust that, either plating a gold leaf on the surface or applying a platinum layer using the impregnation-reduction method should be used. For this study, the chemical impregnation-reduction method was used. The same process was also used for the reference 3D printed sample

The impregnation-reduction process adopted consists of the following:

Hydrolysis

The hydrolysis process consists of two steps:

1. Hydrolyzing in solution of 15 wt% KOH- 35 wt% DMSO- 50 wt% deionized water at 75°C

Rate reported 1.3 um/min. 0.5 mm would take 4 hours and maybe a bit longer [66]

2. Clean membrane by soaking it in three successive baths of deionized water at 75°C for 30 minutes each

Surface treatment

3. Membrane is soaked in 3 wt% H_2O_2 solution at 65°C for 45 minutes
4. Membrane is soaked in deionized water solution at 65°C for 15 minutes
5. Membrane is soaked in 15wt% H_2SO_4 solution at 65°C for 45 minutes to clean and convert into acid form
6. Membrane is soaked in two more successive baths of deionized water at 65°C for 45 minutes

Electrode plating

In this process, platinum ions are chemically reduced to platinum atoms on the membrane surface:

7. Membrane is soaked in 0.02 molar solution of tetraamineplatinum(II) chloride hydrate (Pt(NH3)4Cl2) at room temperature and left overnight
8. Membrane is immersed in deionized water at room temperature. Reducing agent (NaBH4) is added every 30 minutes for three hours while slowly increasing the temperature to 65°C
9. Soak samples in two successive baths of deionized water at 65°C for 45 minutes each to clean them
10. Check surface resistance using a 2 probe multimeter

If the surface conductivity is above 5 Ω/cm, the process starting from step 5 to 10 is repeated.

The same process that was conducted for the reference membrane was used but for the DAP sample but with adjustments added to take into account the influence of the Ruthenium Dioxide electrodes. First, the hydrolysis rate is reported at 1.3 um/min as previously mentioned [66]. However, this rate was studies for a Nafion membrane only, meaning it did not consider the roughness of the surface from the 3D printing neither the presence of a Ruthenium Dioxide- Nafion mix. In their study, they reported that some samples were not fully functionalized and had to leave samples for longer to achieve a better result. For that reason, the hydrolysis process was extended, the membrane was placed in the DMSO/KOH mixture for 6 hours according to the final obtained thickness of 0.85 mm for 4 hours at 65°C, it was then placed at room temperature and left over night. It is hypothesized that the increased roughness and possible poor mixing of Ruthenium Dioxide- Nafion could lead to a slower rate of penetration into the membrane

CHAPTER FOUR

RESULTS AND DISCUSSIONS

4.1. Extrusion process

Extrusion was performed at 220°C. The mold temperature was kept at 185C. The filament extruded had a diameter of 1.6 mm (no swelling) in agreement with previous simulations. One should note that the length of filament in simulations was 7.5 cm. This is important when considering gravitational effects. As the length of the extruded filament increases, the forces exerted on the nozzle exit due to the extrudate weight increases. Beyond 7.5 cm, necking starts to occur, and a reduction of diameter is observed instead of swelling. This was observed both experimentally and in simulations.

To obtain a longer filament without risking any necking issues, a small plate was fixed to the frame at a distance of 7.5 cm from the nozzle. The filament would deposit on the plate and no additional weight would be exerted.

The weight of the filament played a role analogous to the drawing mechanism in other filament machines. The effect was less pronounced compared to the ambient temperature as the filament diameter was relatively constant across the entire length of the filament. In some cases, the tip displayed small selling with a diameter of 1.7 mm. This would happen mostly in cases with rapid extrusion as simulation were conducted for low flow rates.

4.2. DAP mixing and polymer-metal filament extrusion

To 3D print the electrodes, a filament of polymer-metal mix must be obtained. Common methods in metal and polymer-metal feedstock preparations usually use a double screw extruder to achieve proper mixing. There are multiple types of double screw extruders based on the motion, the importance however lies in the shearing forces produced that generate heat due to frictions and help with the mixing process. The produced feedstock would then be used in a single screw extruder arrangement since it provides better extrusion stability but does not provide good mixing

These arrangements prove to be expensive and form a complex pipeline that is justified only in the case of large-scale processes. In addition, proper mixing of a polymer metal mixture before extrusion leads to a more homogenous mixture. Inspired from the findings and given the plunger extruder system currently employed, the Ruthenium Dioxide powder was mixed with some Nafion pellets under high temperature heating to form a homogenous mixture. The resulting mix would be cut into small pellets and placed in the extruder to obtain the required filament.

Optimal volumetric loading Ruthenium Dioxide mix in the electrodes was found to be 42% for optimal IPMC actuation [45]. Although the electrodes would be very thin and would not require much material to fabricate, there is a buffer region of 8-9cms between the driver gears and the opening of the liquefier that needs to be taken into consideration when calculating the required filament length. Assuming a filament length of 20 cm to be used for multiple trials and an average diameter of 1.7mm, the volume required would be 453.9612 mm^3 or 0.4539612 ml. The density of Ruthenium Dioxide is 6.96 (g/ml) and that of Nafion is approximately 2 (g/ml), resulting in a target mass of 1.327g and 0.5266g respectively. The detailed values are shown in the table.2 below:

Table 2-Quantities required for polymer-metal mixture

	Density (g/ml)	Target volume (%)	Mass (g)	Volume (ml)
RuO2	6.96	42	1.32701938	0.190663704
Nafion Precursor	2	58	0.52659499	0.263297496
Total				0.4539612

A plate was placed on the top of the current thermal mold with an NTC 3950K temperature sensor attached to it. A small piece of fiberglass was placed on the top of the sensor to get more accurate readings of the surface temperature and avoid any form of convection and radiation with the surrounding environment. The mixing bowl, in the shape of an aluminum cylinder block, was placed on the plate. Using a mixing bowl was essential since the plate had to be covered with fiberglass to insulate properly and reach high temperatures. As a result, the mixture could not be placed directly on the plate since threads and debris of fiberglass can easily detach and would contaminate the sample. Another issue was the contact thermal resistance between the plate and the mixing bowl. Reaching temperatures above 240°C required a plate temperature above 300°C with issues in directly controlling the bowl temperatures. As a remedy, the cylinder block was wrapped with nichrome wire that was connected to a DC power supply. A layer of Kapton tape was placed between the nichrome wire and the block to prevent short circuit while an additional layer was placed on top of the wire to electrically isolate it from any possible contact with external objects. Another NTC 3950 100k thermistor was placed on the cylinder surface and wrapped with Kapton tape before wrapping the whole block with fiberglass insulation.

Although the thermistor would measure the bowl surface temperature and not the inside of the mixing area, the temperature was considered uniform enough across the object to deem it acceptable for monitoring the mixing process. The aluminum material is

Alumec, obtained from Wardi steels (local supplier), with a thermal conductivity of 165 w/k.m. Ansys simulations using the transient thermal library showed that under normal operating conditions, the difference in temperature between surface and interior is negligible and thus can be considered with minimal impact on the results.

Obtaining good mixing would require a low viscosity from the polymer for better flowability and metal particle insertion in the polymer matrix during mixing. Thus, a high temperature would be required but care should be taken in order to not reach very high limits. Polymers subjected to high heating temperatures for an extended period can be annealed and the same temperature would have to be reached in order to melt it again

Based on the findings of [59] the viscosity of Nafion precursor decreases as temperature is increased, with values shown up until 250°C in figure.8

Figure 8-Variation of viscosity in function of temperature taken from [59]

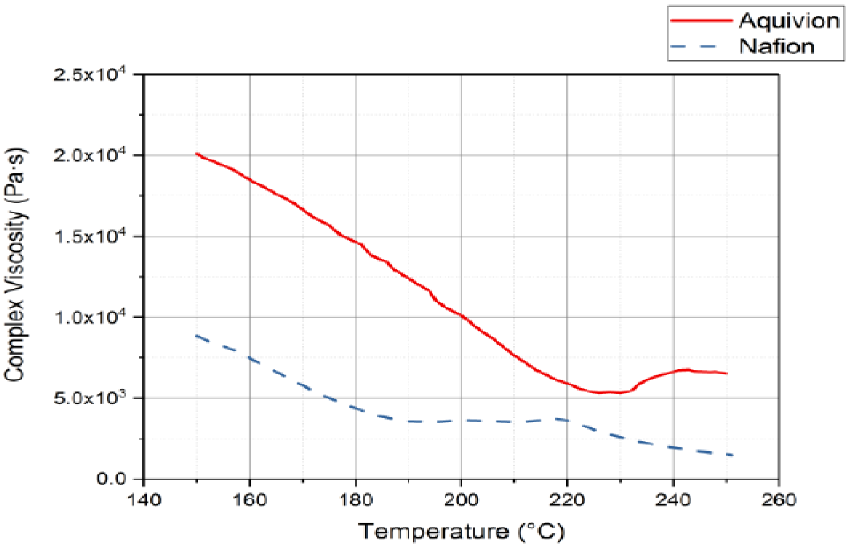

To achieve a better mixing, the temperature was raised slowly in the mixing bowl to a value of 275-280°C. The plate temperature was maintained at constant temperature of 200°C and was controlled by switching the heating units inside using a solid-state relay. On the other hand, the control of the mixing bowl was achieved by connecting the nichrome wire to the DC power supply via an electromagnetic relay. In both cases, control was achieved via a bang-bang threshold method. The voltage supplied via the power supply was increased manually every 5-10 min to achieve a slower rise in temperature. Relays and sensors were connected to an Arduino Uno that was interfaced on Matlab, this made recording and saving of the sensor output easier for analysis. The sensors were samples at a frequency of 1 Hz considering that serial connections via Matlab do not achieve very fast sampling rates

The mixing process took around 38.6 min in total, the sensor values are shown in figure.9 for a range spanning 1072 seconds to 2304 seconds:

Figure 9-NTC 3950 100k thermistor temperature measurements

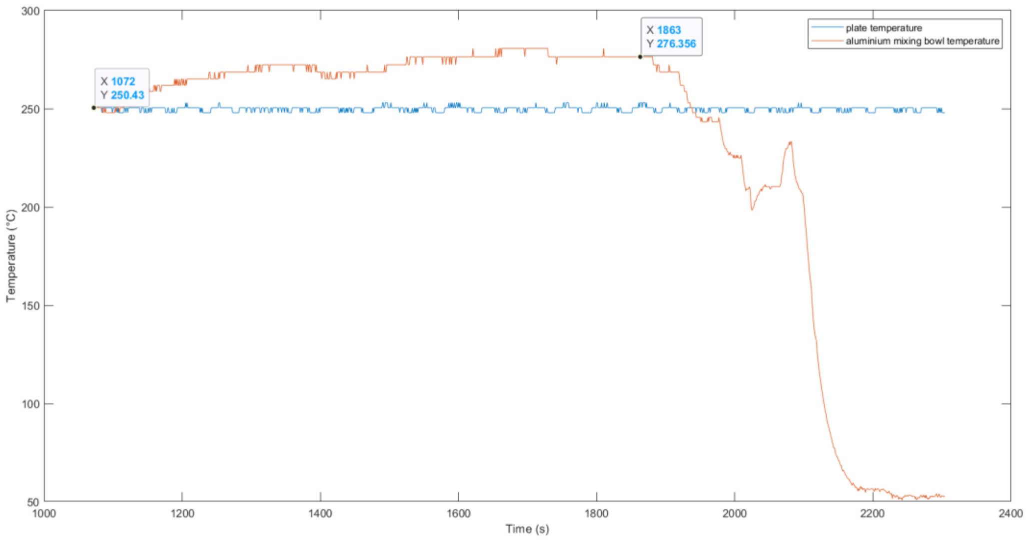

It is noticeable that the plate temperature was kept at a constant value with minor fluctuations in terms of magnitude. The mixing bowl temperature increases slowly to reach a maximum of around 280°C for a brief period of time. In the meantime, the Ruthenium Dioxide was introduced in small quantities gradually and stirred manually using two stainless steel rods. The final mixture achieved was homogenous in nature with no apparent concentrations of Ruthenium Dioxide on the surface as seen in figure.10

Figure 10 -Nafion/Ruthenium Dioxide mixture

Since a homogenous mixture is required, a second mixture was prepared but more and faster stirring was used during the process. Surprisingly, the Nafion degraded leaving only the metal powder in the mixing bowl. This was unexpected, given that degradation of Nafion starts at 300°C and noticeable mass change occurs around 400°C[59]. However, the degradation is reported for a strain rate of 1(s^{-1}), therefore higher strain rate could induce faster degradation (need to find reference). This casts further doubt on the usage of twin extruder as mixing mechanism for later preparation.

To solve this issue and conserve as much material as possible, the mixing strategy was altered. The bowl temperature was kept at 220°C at first, with the Ruthenium Dioxide powder introduced gradually. The Nafion mixture was first pressed against the bowl and left for 1 min, giving time for the Ruthenium Dioxide to heat up and for molecular diffusion to occur. After that the mixture is gently mixed with the stainless-steel rods. The process is repeated multiple times until no metal powder is loose in the bowl, in that case more metal powder can be added. Once the quantity is completely introduced, the temperature is raised to 230°C while repeating the process several times until no loose powder is visible on the surface of the mixture or in the mixing bowl.

Large shear forces are expected at the entrance of the extruder die. Given the decent metal volumetric load of the mixture, the temperature was raised to around 220 °C for the extruder. Figures.11 and 12, show the temperature variations for the inside of the extruder and the plate across time with a sampling frequency of 1s.

Figure 11-variation of extruder temperature with respect to time

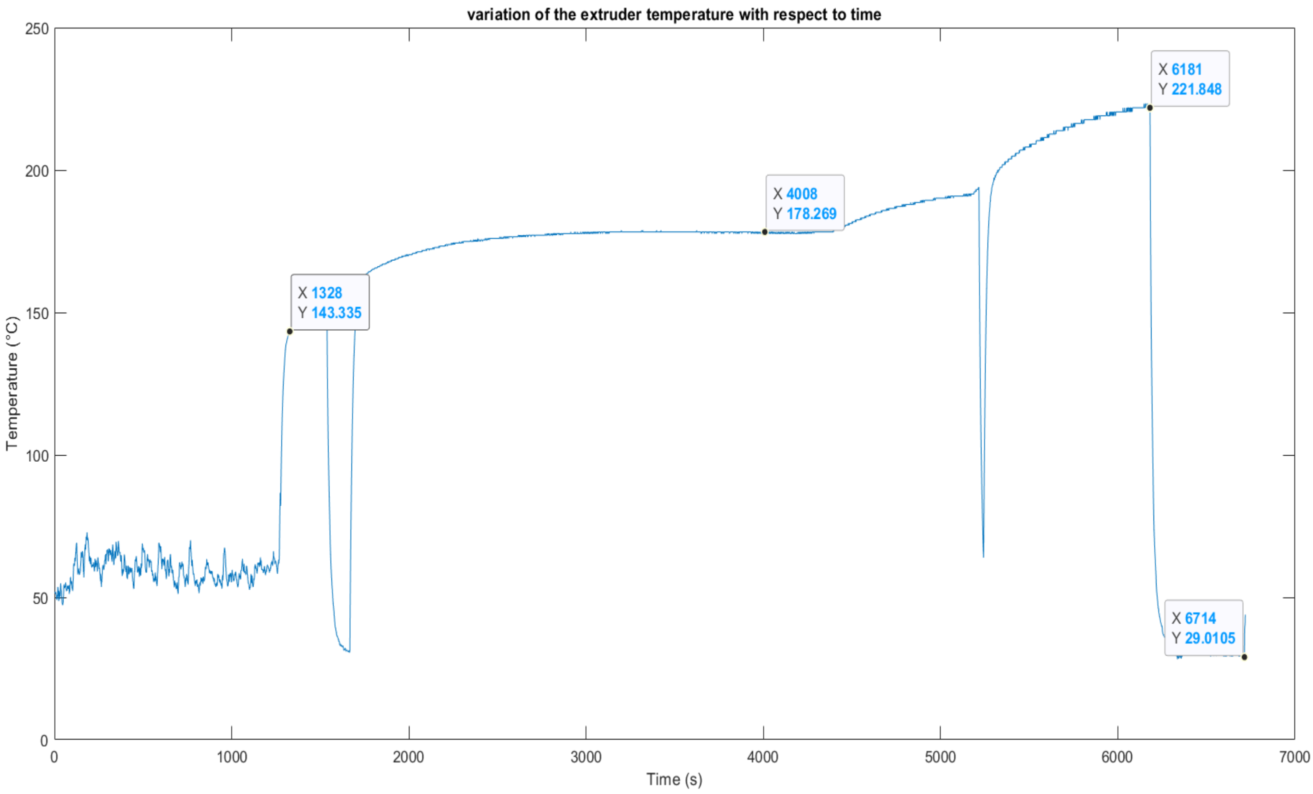

The material was left at around 175-178°C for a large period of time to remove moisture before melting of Nafion and avoid the formation of traces of HF gases. The sudden drop of temperature at the end of figure.11 corresponds to the removal of the sensor to start extruding. At these temperatures, the filament displayed noticeable die swell and other rheological effects. The beginning of the filament had a diameter of 1.9mm, this diameter drops to around 1.7 mm after 2 cm of length and stays constant for 5 cm before starting thinning and reaching a diameter of 1.5mm after around 12 cm.

These values are consistent with the values obtained for a Nafion filament, displaying thinning due to elongation of filament under gravity. The results however span a wider range of filament indicating that the material was somewhat more resistant to rheological effects, which is in accordance with the finding of on extrusion of polymer filled composites. The comparison is however not reliable for this case as the extrusion process was done manually by turning the threaded plunger. Variations in extrusion speeds could lead to large variations of shear rate and affect the die swell phenomena.

Throughout the process, the mold was kept at 185°C, as seen in figure.13, to promote slow solidification of the filament and allow for thermal motion and diffusion to realign the elements as previously mentioned

Figure 12-Variation of plate temperature with respect to time

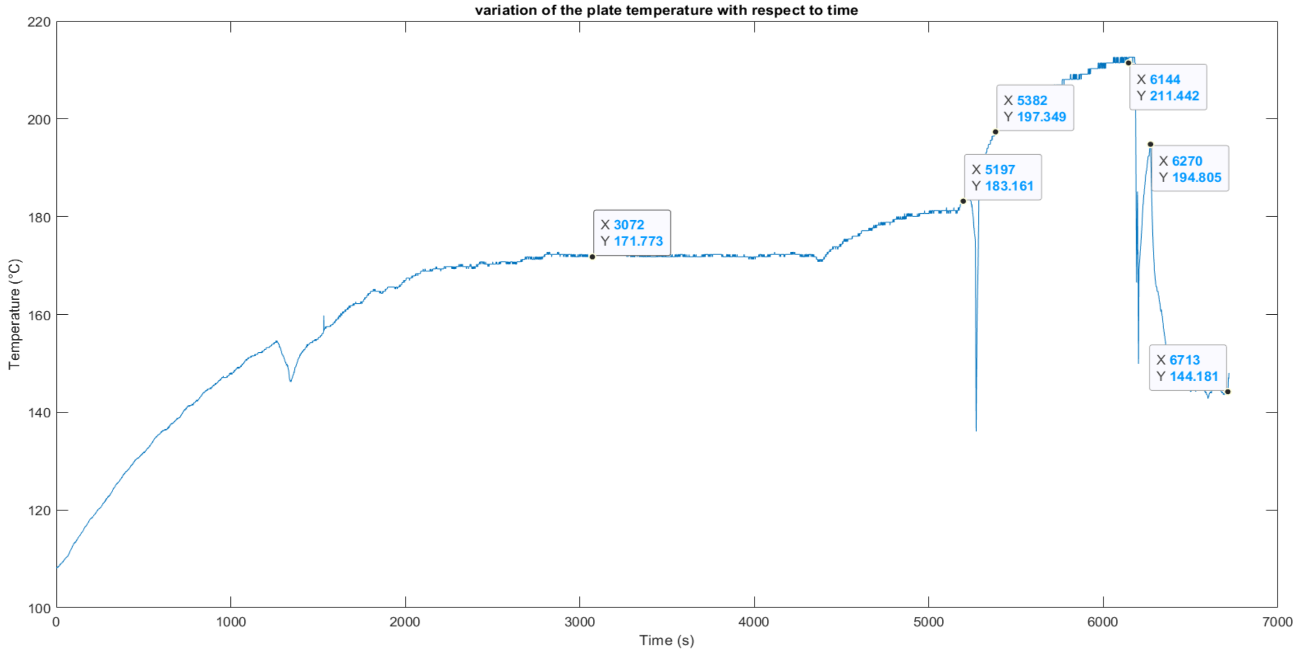

Figure 13-Variation of thermal mold temperature with respect to time

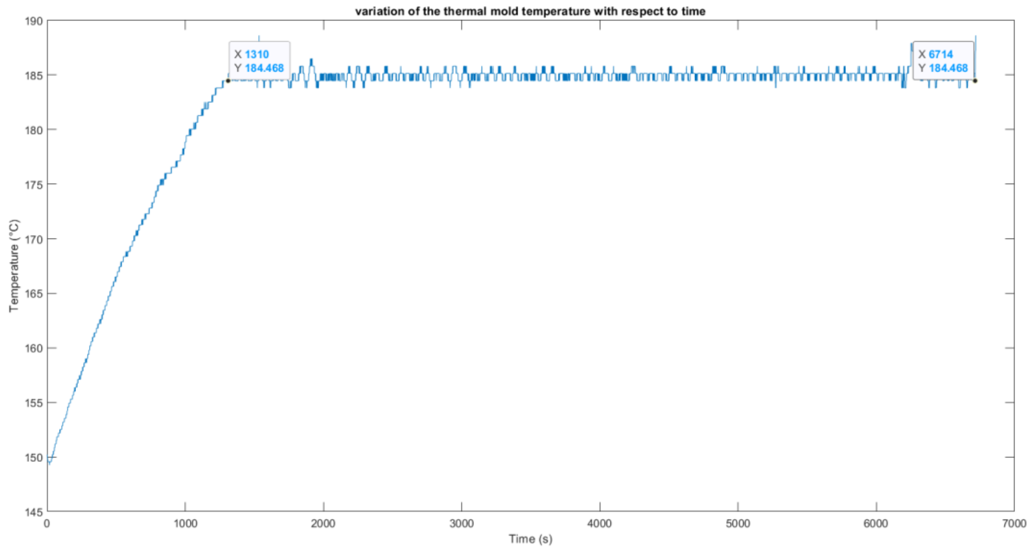

The filament produced was around 20cm long with minor losses during the extrusion process. In order to test it, it was mounted to the 3D printer with the 1.5mm region removed to avoid issues of buckling. It is expected that the added Ruthenium Dioxide will improve mechanical properties, making the material easier to print. However, the degree of this improvement would require tensile tests however to validate. The temperature of the extruder was raise to 285°C and the filament was manually purged at a rate of 1 mm/s. There was a noticeable delay in filament extrusion, the exiting filament had sometimes transparent regions with few blackspots inside. This could indicate either separation of Ruthenium Dioxide from the polymer matrix possibly due to inappropriate mixing or to partial clogging of the nozzle inducing larger shear strains.

To remedy those issues, the filament was cut again to pellet size pieces and placed inside the plunger for a second extrusion. The nozzle of the 3D printer was also replaced, a 0.8mm hardened steel nozzle was used. It was preferred instead of the 1mm used in their experiments in order to have a better resolution and control of extruded quantity for printing very thin electrodes.

For the second extrusion, the temperatures of the plate and plunger were limited to around 200°C. The mixture inside is expected to be at 190-195°C and allows testing for solid state extrusion. The temperature variations are shown in figures14 and 15.

Figure 14-Variation of plunger temperature with respect to time

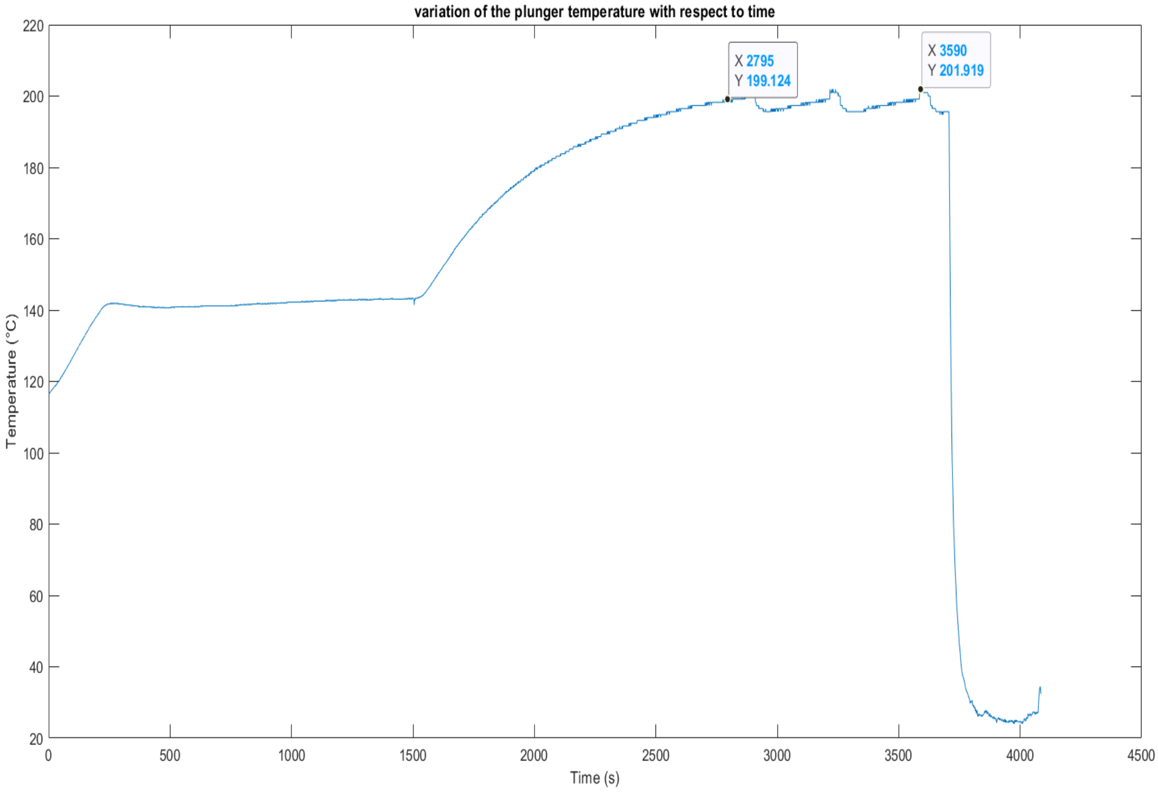

The resulting filament had a smooth surface, with no apparent shark skin or discontinuities, and was flexible enough to bend. The diameter was 1.6 mm and consistent across the entire length, indicating the absence of die swell and the potential success of solid-state extrusion

Figure 15-Variation of plate temperature with respect to time

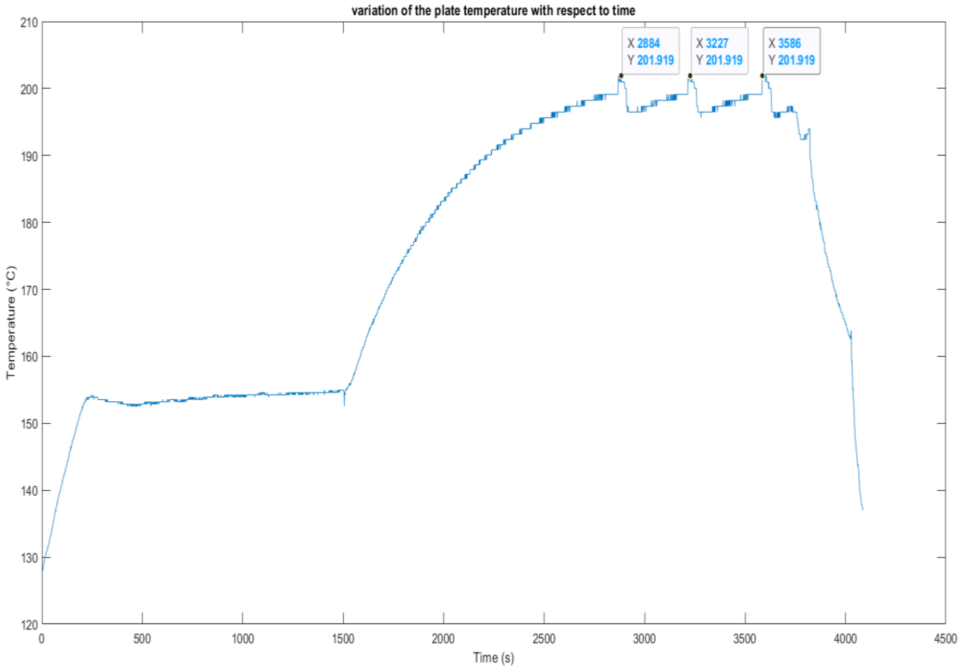

4.3.3D printed samples

Given that the printing process was not calibrated on Nafion filaments due to low available quantities of the material, the sizes of the obtained membranes differed slightly from the original design with final sizes of 14mm x 5mm x 0.5mm and 13mm x 4.5mm x 0.5 mm for the two membranes produced and used later in the study, as seen in figures 16,17 below:

Figure 16-Membrane 1

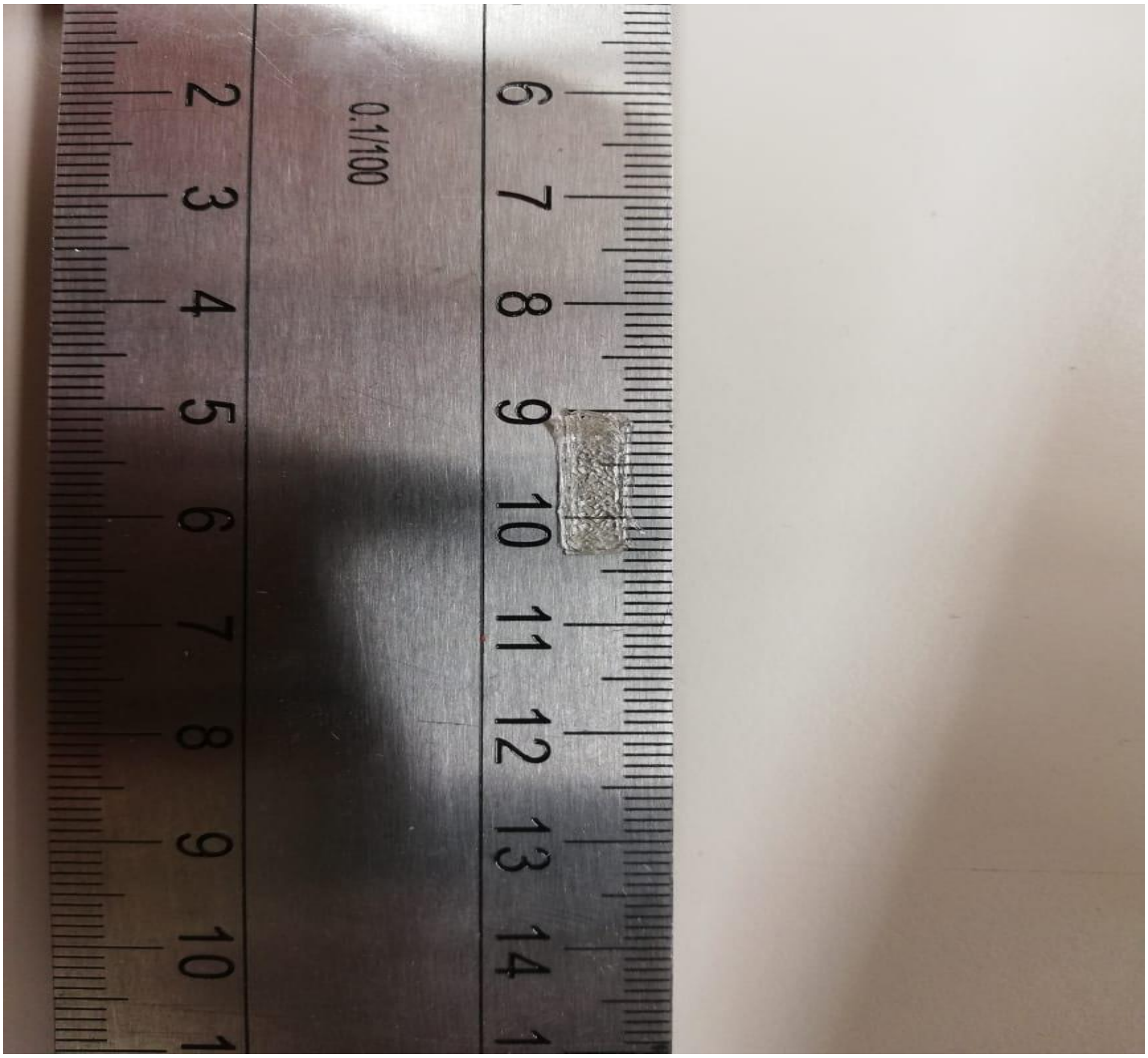

The infill density was set to 100% and the pattern was chosen to be a grid form. Nonetheless, some voids are noticeable. This is due to the fact that the 3D printing process is a discrete and discontinuous process. These areas occur from possible low adhesion between deposited layer of lines of material.

Figure 17-Membrane 2

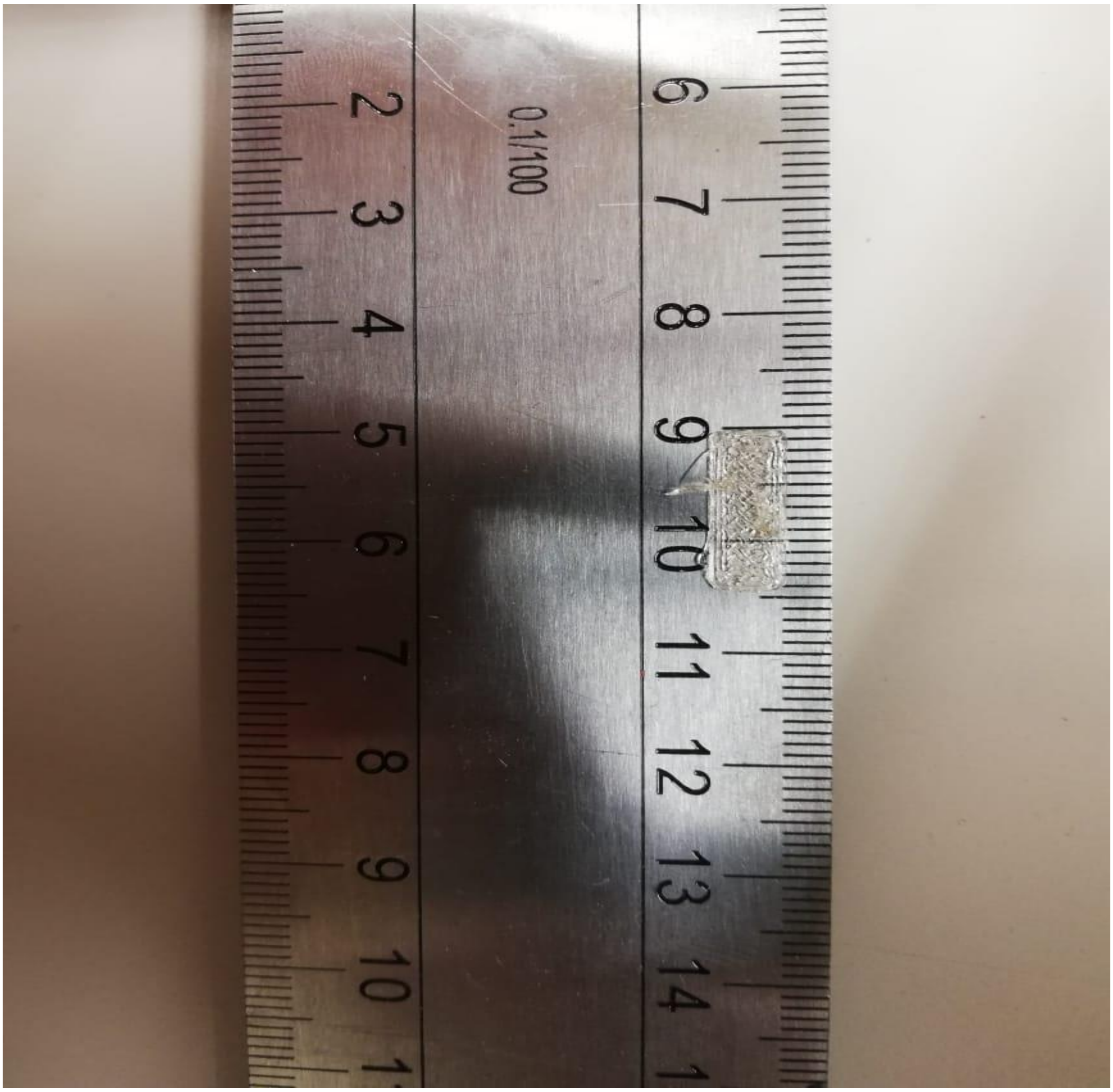

A first trial to purge the metal/polymer feedstock through the nozzle showed signs of a delay in extrusion. Also, the Ruthenium Dioxide metal particles were agglomerating and separating in some locations of the extruded filament. The delay and separation were indication of partial clogging of the nozzle. A hardened steel, 0.8 nozzle was chosen instead. Increasing the nozzle size reduces back pressure and is used for flexible. It could also solve the issue of partial clogging. Care should be taken regarding the resolution as increasing the nozzle size would lead to wider and thicker lines.

The electrodes were designed to be approximately the same size as the membrane previously mentioned but with 0.1 mm thickness instead. A few millimeters were removed to consider possible excessive spreading of the material due to a larger nozzle. The final geometry used was 13mm x 4mm w 0.1mm. Although the resolution of the stepper motor is around 0.025 mm in the Z-direction, there were resolution issues when printing thicknesses below 0.1mm when investigated used PLA filaments.

The main issue to solve when printing on top of an existing structure is the layer adhesion. Studies report the main factors affecting layer adhesion, either bed adhesion or interlayer adhesion, are nozzle temperature and surface deposition temperature. Higher temperature induces better molecular diffusion and thus better adhesion. The layer height can also help, with a low layer height promoting wider lines and better contact. Also, the bed pate temperature cannot be heavily increased to preserve the geometrical integrity of the original membrane, with Nafion transitioning to fluid like states at around 200°C.

Simulations of the heating process showed that for thin membranes such as the ones used, a negligeable difference of around 3-4°C should occur between the top of the membrane and the bottom heated surface.

Figure 18-Simulation of Nafion membrane on heat bed

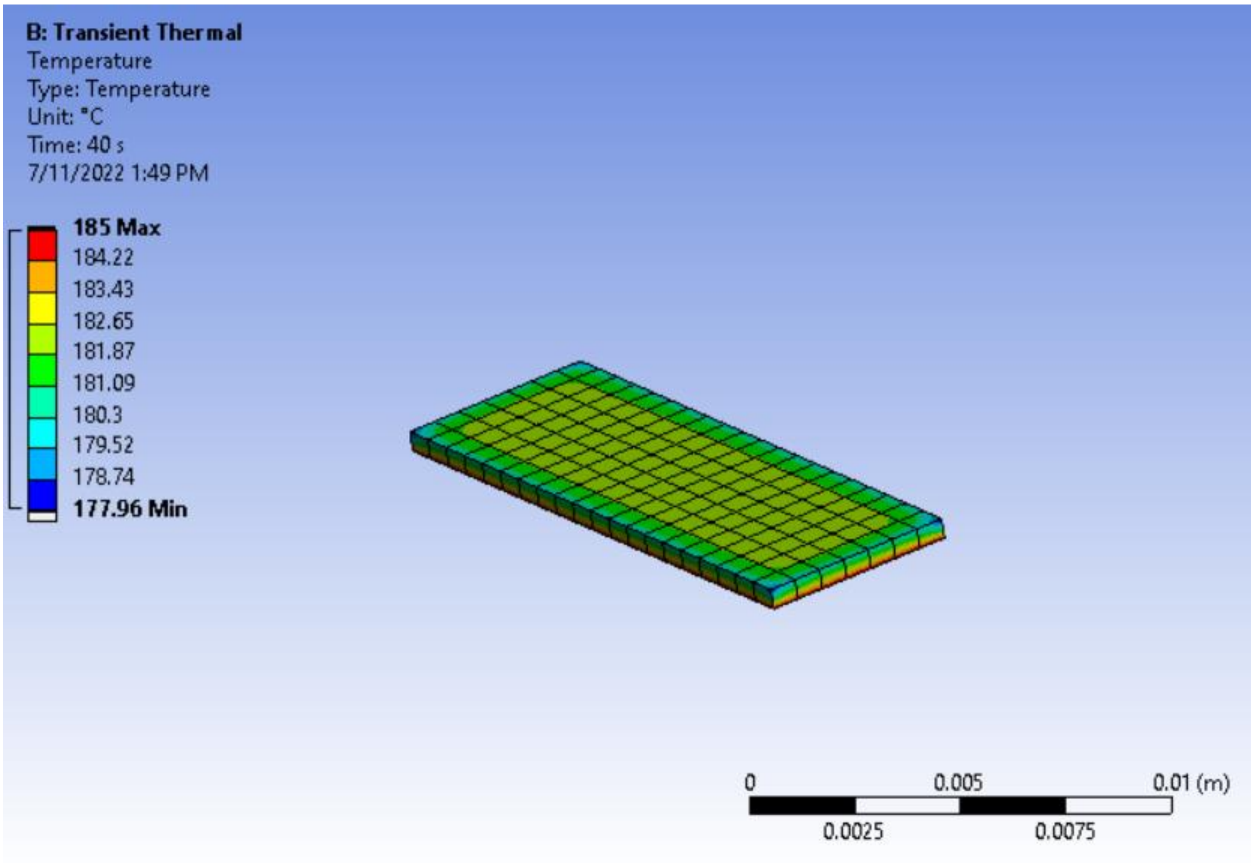

A constant temperature of 185°C was imposed on the bottom layer and an average heat transfer coefficient of 10 w/m^2.k was assumed for the convection process.

This was confirmed experimentally as well. A membrane made out of PLA was printed and taped to the heat bed using Kapton tape. A NTC 3950 100k thermistor was attached on the top surface of the membrane with another measuring the temperature of the lower heat plate. Since PLA melting temperature is around 140°C, another Ansys simulation was run using PLA for a heat bed temperature of 125°C and found the surface temperature of the membrane to be 122-123°C. The temperature measured by the temperature sensor for a heat bed temperature of 125°C is shown below:

Figure 19-Pla membrane surface temperature

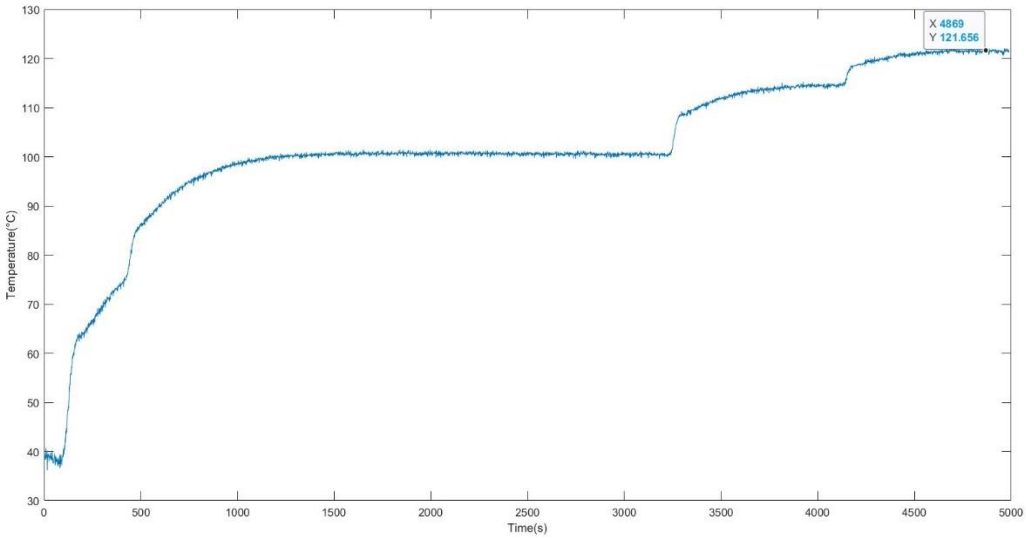

This confirms the initial suggestion that the temperature difference the top of the membrane should be suitable for printing.

The same printing settings were used, with the flow multiplier decreased to 1.3-1.4. this indicates that the Ruthenium Dioxide filament was slightly easier to 3D print. The issue was with material oozing out of the nozzle. As the nozzle diameter was larger, the back pressure was smaller, and material was flowing out of the nozzle easily due to gravity even if the filament wasn't being extruded. This led to larger discontinuities, mainly at the start of the print. The problem was mitigated by slightly purging the filament directly before the start of the print but remained to some extent.

The obtained electrodes showed good adhesion and geometrical integrity when printed directly on the membrane.

4.4.Rheology simulation

Numerical optimization was carried out for shear values between 0.1-10 s^{-1}, which the range measured in [29].

The process was repeated 10 times to guarantee the repeatability of the results. The value of the optimal mobility factor was found for each shear rate with an increment of 0.1 s^{-1}

Figure 20-Results of numerical optimization for mobility factor

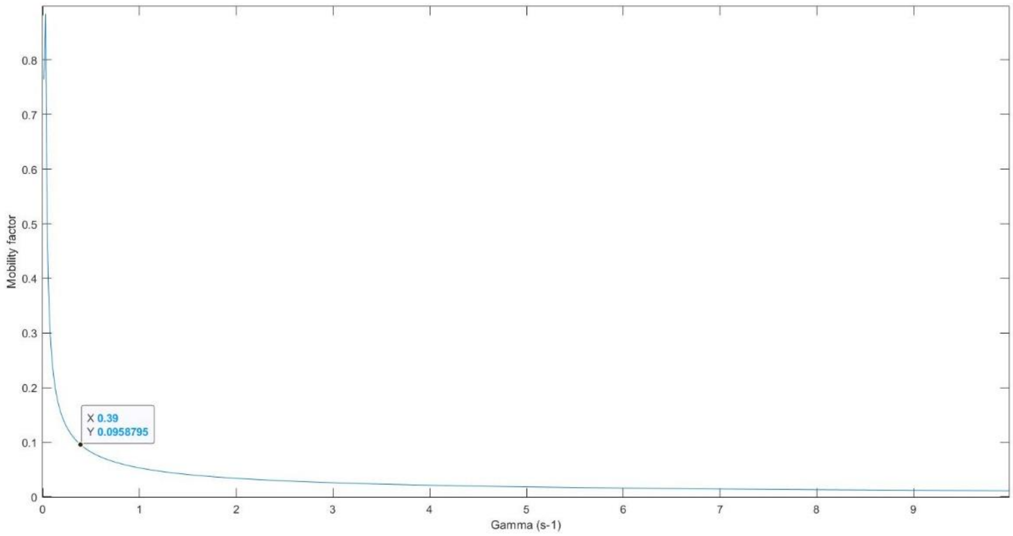

The results vary drastically at the small shear rates but seem to become constant after a shear rate of 0.4 s^{-1}. An average value of 0.03 was used for the mobility factor in the Polyflow simulations which is the average of the later constant stage on the curve.

PolyFlow simulations were carried out with the Nafion thermal properties and Giesekus model factors appropriately selected. The thermal properties of Aluminum A4043 were also used for the conduction in the plunger.

Figure 21-Temperature profile from the Polyflow simulation

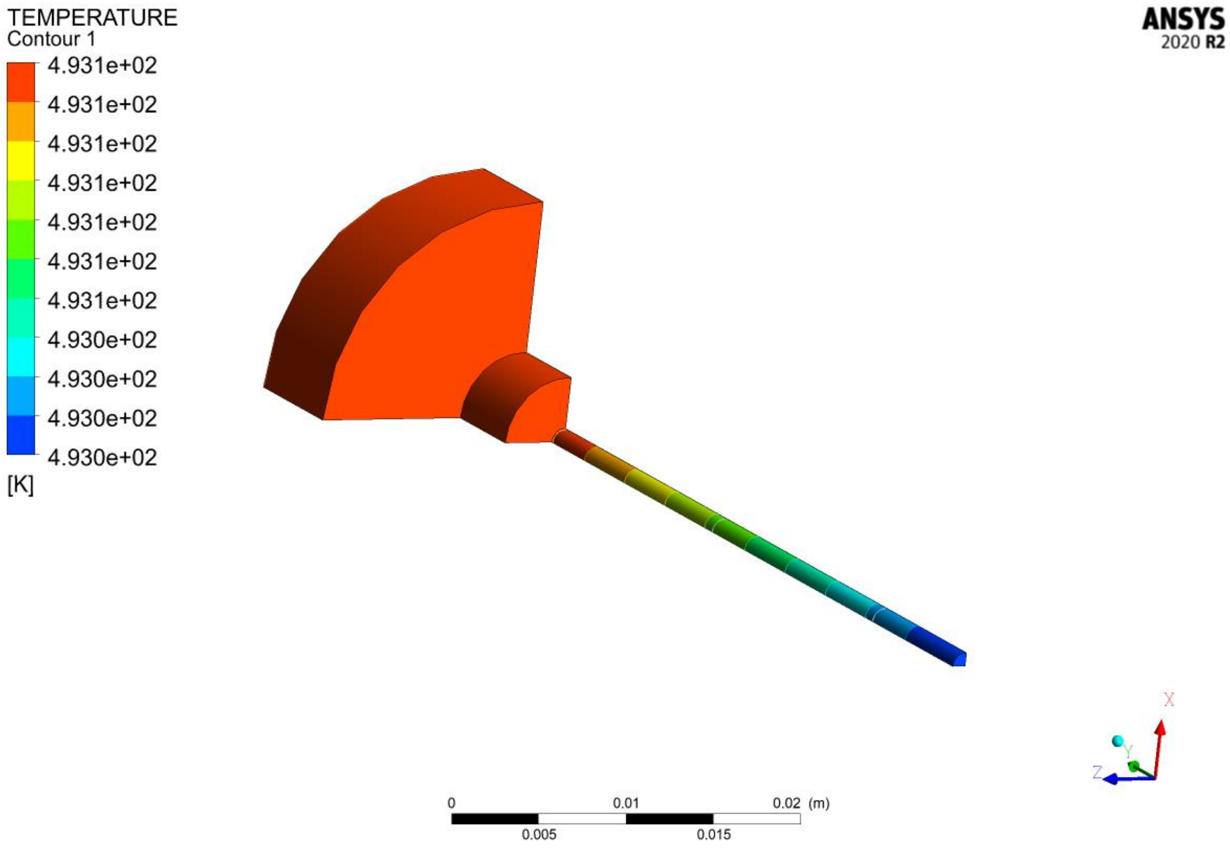

For a temperature of 220°C and a plunger rate of almost 2mm/s, corresponding to the input values for the lab experiments, the simulation resulted in an average diameter of 1.597 mm and no die swell which is consistent with the results obtained in the experimental trials.

Figure-21 shows the temperature variation given the 185°C ambient temperature inside the mold. The obtained filament can be seen with no apparent distortion on the cross-section indicating no die swell or changes.

4.5. Chemical activation

For the first membrane, the full chemical process was conducted, and 4 layers were plated on the surface. The resulting surface resistance was tracked throughout the process and the results are shown in table.3 Below:

Table 3-Plating progress of reference 3D printed membrane

Number of Layers	Surface resistance (Ω/cm)
1	17
2	7.5
3	6
4	3.125

For the second membrane, the presence of Ruthenium Dioxide printed electrodes would affect the rate of hydrolysis. As reported in [65], the hydrolysis process moves inwards inside the membrane at a rate of 1.3 um/min. however, the printed electrode texture might affect this rate. In addition, some studies showed that sometimes the membrane is not fully hydrolyzed and even left it overnight. Based on that, the second membrane was left overnight at room temperature to guarantee a full functionalized membrane. The chemical plating process was then repeated until the surface conductivity dropped below 5 ohm/cm

The process was conducted normally afterwards. The resulting surface resistance varied between the sides. One side displayed a surface resistivity ranging between 25-40 ohm/cm while another side showed values between 50-70 ohm/cm. In addition, the measurements differed based on the layer of Ruthenium Dioxide chosen reaching almost 100 ohm/cm in some cases. Since 3D printing is a discrete process, there were distinguishable layers and some voids apparent in small regions. This could be adjusted during the 3D printing process by increasing the overlap between the lines. This could also be increased by increasing the flow rate or lowering the layer height to make the lines thicker. However, for the given 3D printer used, the layer height used was already below what is reported in practical case usages as acceptable layer height.

To solve this issue, the plating press was repeated for 4 layers, high anisotropy was still present after that with surface resistivity measured varying between layer lines chosen. The average surface resistance is reported below:

Table 4-Plating progress of Ruthenium Dioxide 3D printed membrane

Layer order	First side surface resistivity (Ω/cm)	Second side surface resistivity (Ω/cm)
1	30-50	50-70
2	22.5	34.5
3	13	23.7
4	5-7	14.4

Figure 22-surface resistance measurement for second electrode side

Two points are worth mentioning here. First of all, the surface is highly anisotropic, with sometimes the surface resistance increasing as probe gets closer to each other. This can be traced down to two things: high surface roughness and voids due to 3D printing process, especially that a flexible filament would require a better nozzle with perhaps a higher L/D ratio. On the other hand, the Ruthenium Dioxide/Nafion filament might not be well mixed. As a result, some areas would have a higher Ruthenium Dioxide content than other. It could also lead to poor surface plating conditions and poor penetration into the membrane. There were reported cases were agglomeration of platinum led to poor surface plating by forming larger clusters that blocked further penetration, a similar phenomenon could occur in the current case as well.

Another aspect to investigate is the difference between the two electrodes. The electrode with the worst surface resistivity was printed last. When the first electrode is printed, the membrane is flipped and refixed with Kapton tape. Therefore, it was subject to 185°C temperature for around 10 minutes, the approximate duration of the 3D printing process. This combined with the reasonably high temperature due to printing means the electrode was subject to a thermal treatment where molecular diffusion might have occurred. This could have resulted in a better mixture inside the electrode and a better distribution of Ruthenium Dioxide. The fact that Nafion was successfully extruded using solid state extrusion at 185°C means it is flexible enough to allow some form of diffusion and rearrangement at this stage

4.6.Hot pressed membranes

Obtaining a required thickness consistent of multiple trials, where the pressure was increased slowly each time. For the Nafion membranes, samples were left at a temperature of 220°C for a duration ranging between 5-8 min.

Two rectangular membranes were obtained of size 2 cm length x 0.5 cm width. They had an average thickness of 0.3 mm and 0.1 mm respectively. The surface obtained were highly uniform and smooth with no apparent damage or waviness in the texture

Figure 23-Nafion membrane before cutting

When heat pressing the Ruthenium Dioxide-Nafion mixture, more pressure was required due to the increased stiffness and the process was performed at 230°C instead. Two membranes made of polymer metal mix were obtained with a thickness of 0.1mm. Their dimensions were slightly increased to make the assembly process with the Nafion membrane slightly easier.

Figure 24-Nafion membrane with hot pressed Ruthenium Dioxide electrodes before cutting

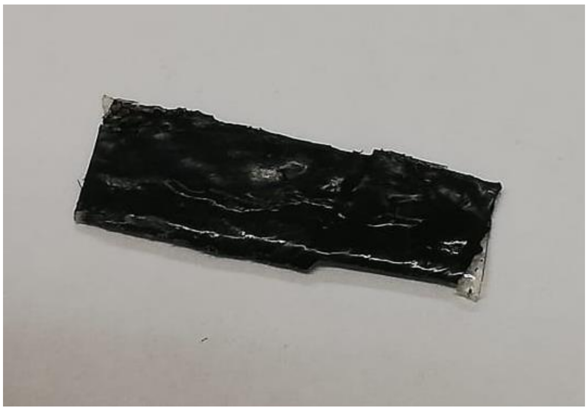

The Nafion membrane with a 0.1 mm thickness was sandwiched between the two Ruthenium Dioxide-Nafion membranes and hot pressed at 230°C for 10-15 min to fuse the three membranes together and obtain Ruthenium Dioxide-based electrodes similar to the DAP process reported. The resulting average thickness was about 0.5 mm, the sample was slightly wrinkled with a non-uniform texture. The increase in thickness could also be the result of swelling of the electrode membranes similarly to the issue of die swell in extrusion since the pure Nafion membranes did not show any sign of changes in thickness.

The process was less straightforward since guaranteeing good adhesion between the layer required high pressure and longer exposure time. Early samples at lower temperatures and shorter exposure times had edges of the Ruthenium Dioxide electrodes slightly detached or not appropriately adhering to the surface. On the other hand, a prolonged exposure led to further decrease in thickness of the Nafion membrane, given its low stiffness compared to the Ruthenium Dioxide electrodes. This is the main reason for the wavy-uneven texture of the surface and increases the risk of short circuit. This could happen in very thin sections of Nafion where direct contact between the electrodes would be possible. There is also the possibility of observing micro short circuit, a concept common in battery separators, where small areas of the electrodes come into contact. In that case, the IPMC might still work but there would be a sever decrease in performance.

4.7.Polymer-metal mixing

The issues and low resistivity that occurred when plating the Ruthenium Dioxide-Nafion electrodes are investigated further. One possible cause are the voids and bad surface finish that could results from the 3D printing process. It can be linked to the quality of the not just the discontinuity of the process.

To investigate the quality of the mixing, hot pressed Ruthenium Dioxide electrodes were placed under a visual microscope to observe the electrode texture.

Figure 25-Ruthenium Dioxide electrode- smooth surface

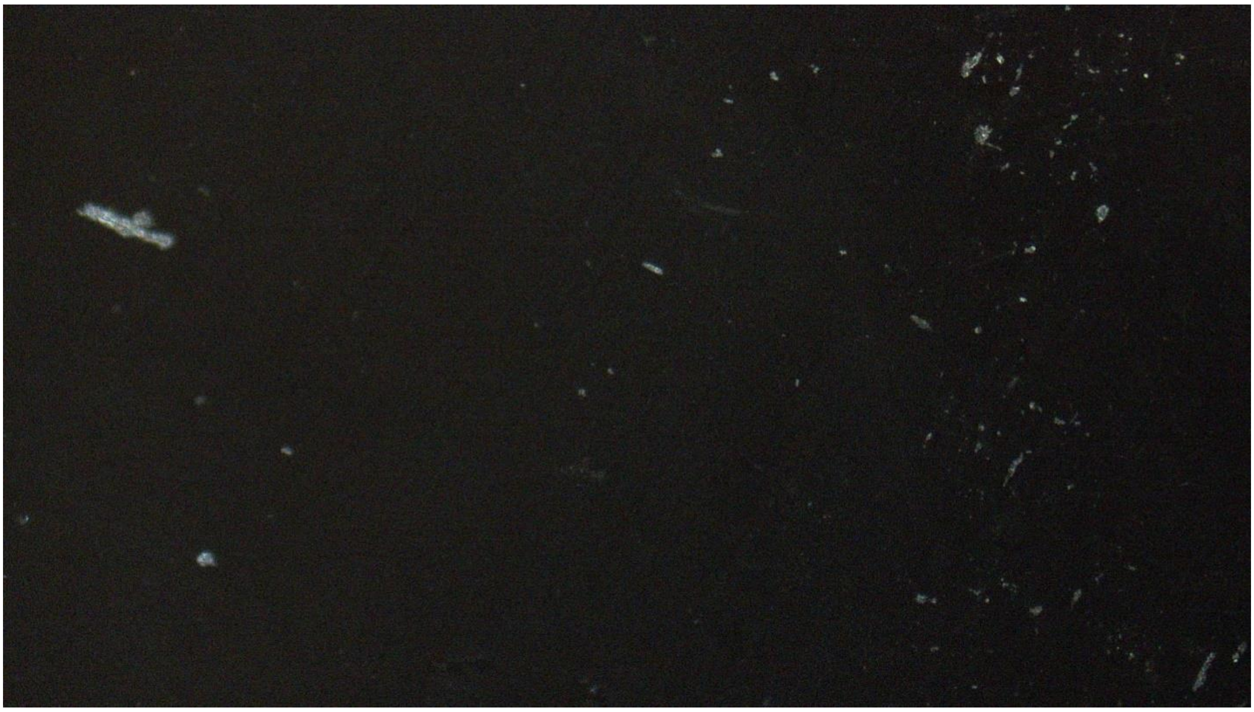

Figure 26- Ruthenium Dioxide-electrode with scrapped surface

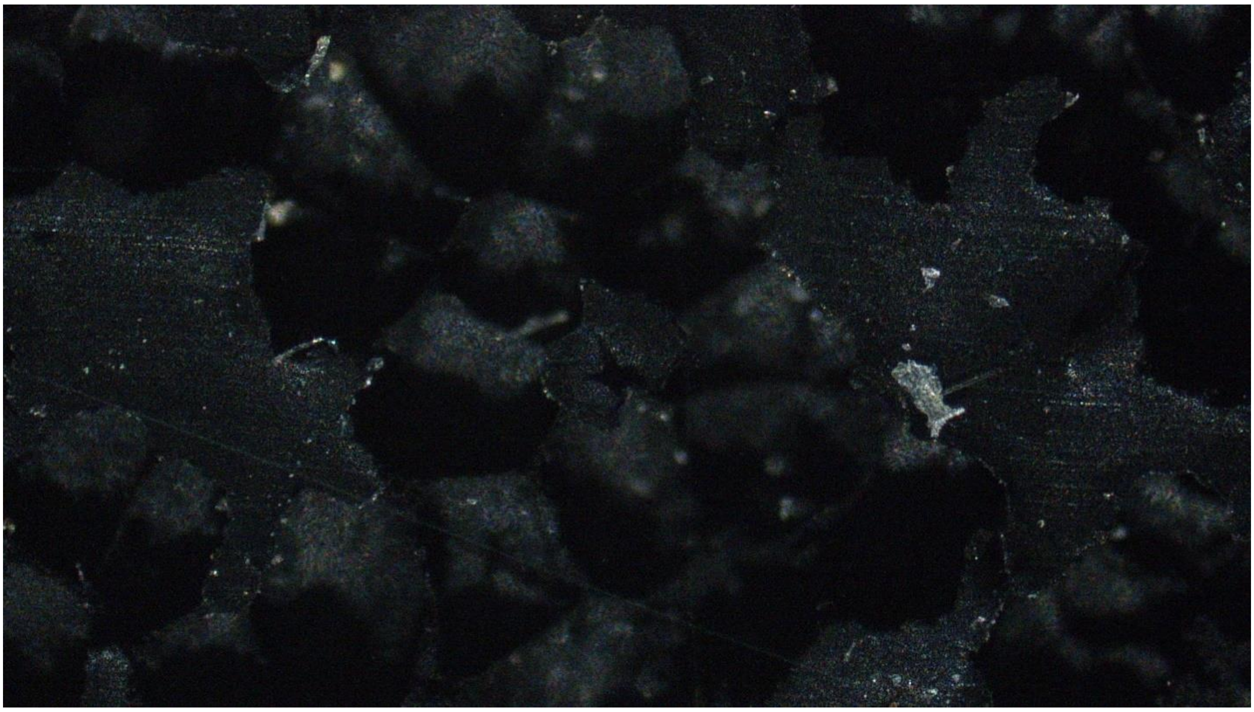

From figure-25, it is clear that the smooth hot-pressed surface shows no indentation. However, the bright spots present highlight a concern that either the samples were contaminated or the Nafion inside is aggregating and did not mix well with the Ruthenium Dioxide powder

A closer look at figure.26 confirms that there is poor mixing in general. The presence of granulation indicates that the Ruthenium Dioxide powder and Nafion are aggregating and there is no homogenous penetration in the polymer matrix.

Figure 27-Damaged electrode from hot pressed sample

Figure-27 shows a damage Ruthenium Dioxide electrode after hot pressing. The cracks available can lead to problem in plating and are due to increased brittleness of the solution which is in agreement with the findings of [89]

A piece of the Ruthenium Dioxide-Nafion mix used for extrusion was cut and the cross section was visualized under the microscope as well.

Figure 28-Filament cross-section

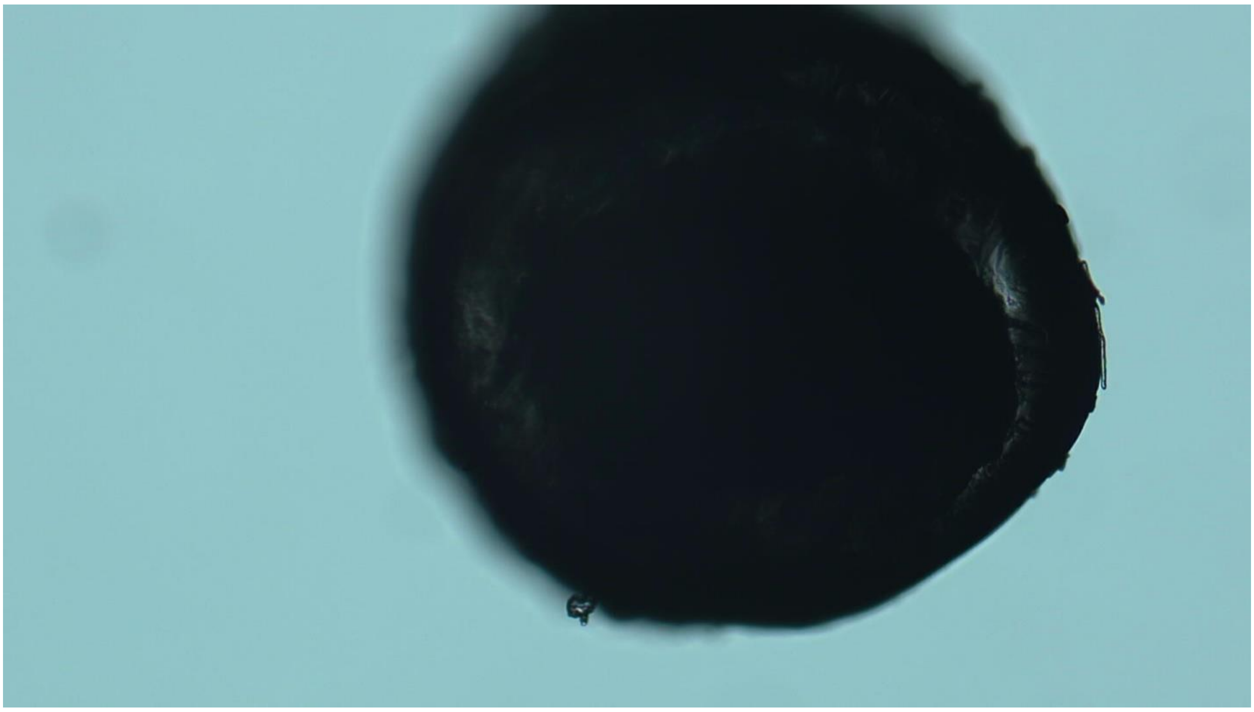

The different coloring on the right-hand side is an indication of phase separation and agglomeration between the Nafion and Ruthenium Dioxide particles

4.8. Actuation results

The actuation experiments consisted of applying a constant 2 volts signal on the membrane and measure the corresponding displacement.

The membrane was fixed using clamps covered with copper tape. Wires were soldered at the end of the tape, connecting it the control circuit.

In order to apply an accurate step input, a 2 volts DC was fed from the DC power supply to the input of an electromechanical relay. The relay was controlled by a NI myRio-1900 through a BJT switch circuit. At the start of recording, the relay is activated to allow the current to pass. The load is directly applied on one copper tape of the clamp.

The other copper tape was connected to the positive input of the voltage amplifying circuit shown in figure-29:

Figure 29-Actuation schematic diagram

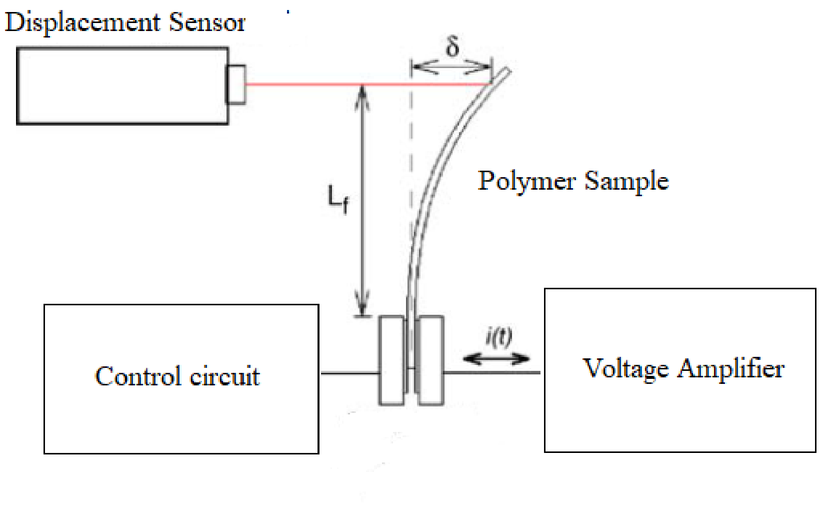

Figure 30-Control circuit

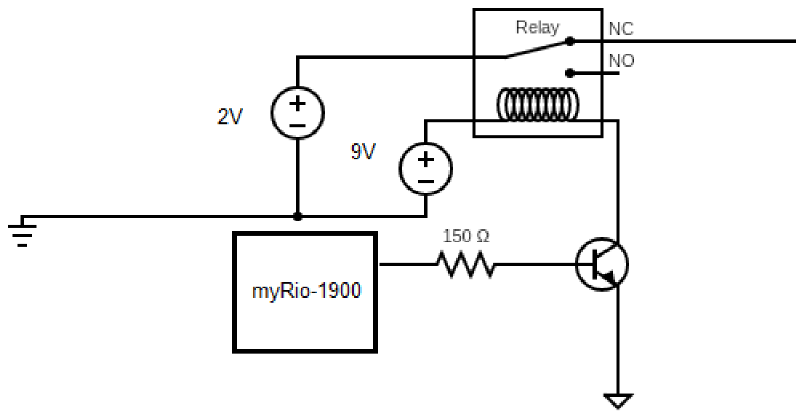

Figure 31-Voltage amplifier

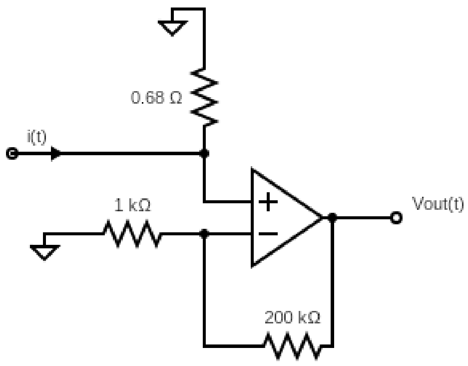

The amplified voltage is calculated using equation.23:

$$V_{out} = 200 \times V^{+} \quad \textbf{(eq.23)}$$

The current is computed based on ohm's law in equation.24:

$$I = \frac{V^{+}}{0.68} = \frac{V_{out}}{200 \times 0.68} \quad \textbf{(eq.24)}$$

The 0.68Ω resistance is the equivalent resistance of a copper wire connecting the positve input to the ground. This value was recorded using a multimeter and verified by calibrating the system on a 200Ω resistance subject to a 5-volt load. To avoid any issues, the system was calibrated by directly placing the 200Ω test resistance directly on the copper tape. The error was measured in multiple trials and a correction factor for the calculated voltage was used to take into account the resistance of the circuit and wires. The DC supply also provides a digital reading of the current drawn from the system, further validating the response of the voltage amplifier

The output of the amplifier is recorded using the myRio and the current value is converted by applying ohms law on the 0.68 Ω resistance using the actual voltage.

All three values: voltage, current and time are recorded using the myRio and saved as excel files that are recovered at the end of the experiment.

Microtrak™ 3 Laser Triangulation Sensor was used to measure the tip displacement. The laser is placed 30cm away from the membrane and positioned such as the line of site of the sensor is perpendicular to the length of the membrane in a cantilever configuration.

Since two devices were used for recording data, results were identified by comparing time stamps of the resulting excel files.

All three membranes, hot pressed, 3D printed and 3Dprinted-DAP, were subject to the same experiment. The membrane is positioned firmly between the clamps in a way to have it perpendicular to the laser beam. Using a brush, water droplets are supplied before the experiment to ensure proper hydration. In cases where a duration larger than 10 seconds was expected, excess droplets were deposited on the surface.

After calibrating the laser to a reference position, a 2-volt step signal is applied. The duration was around 6 seconds for the hot-pressed sample, 4 seconds for the 3Dprinted-DAP sample and 10 seconds for the 3D printed sample.

The results are shown below with subplots of the displacement with the corresponding current and voltage signal recorded.

Figure 32-response of 3D printed sample with impregnation-reduction plating

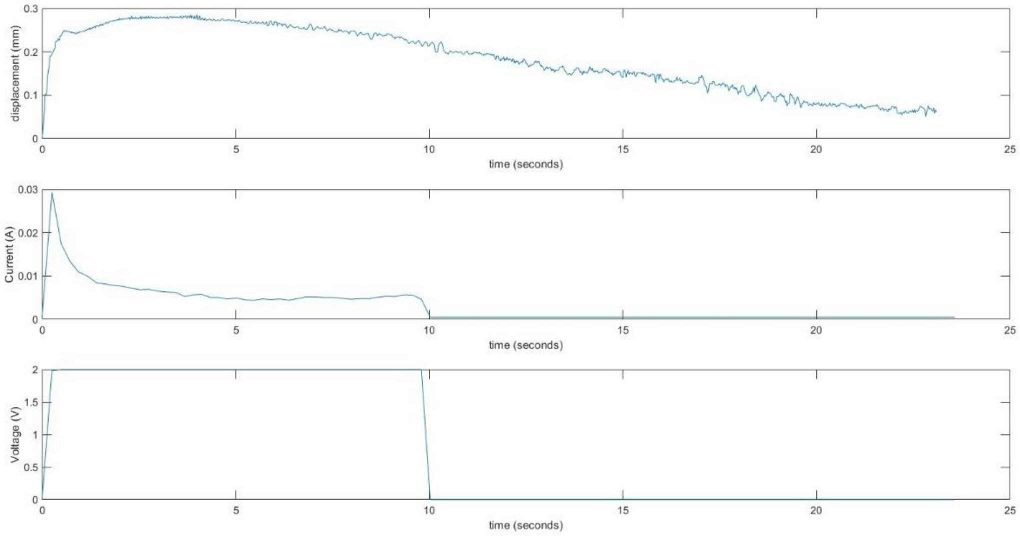

The 3D printed samples plated using the impregnation-reduction method achieved a displacement of approximately 0.29 mm. This was achieved with a free length of 1 cm.

As for the 3D printed sample with Ruthenium Dioxide electrodes, the response was an order of magnitude lower as seen from Figure.33:

Figure 33-response of 3D printed sample with Ruthenium Dioxide electrode

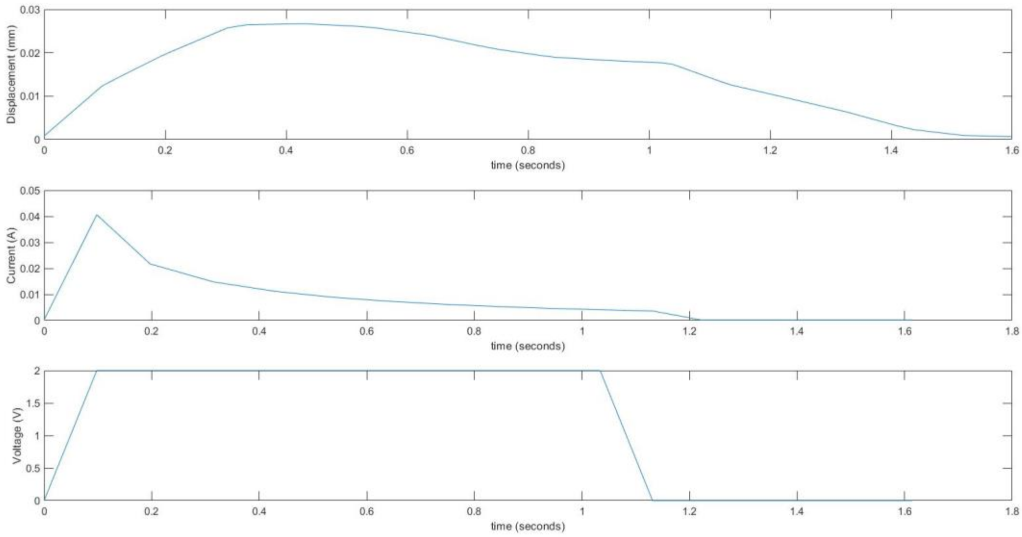

The maximum displacement was around 0.0264 mm. The response is lower than expected. keep in mind that the membrane with Ruthenium Dioxide is thicker in total and with relatively thick electrodes (0.2mm) compared to the plated sample (in the order of μm). This leads to a very large stiffness that is detrimental to motion.

The results for the hot-pressed sample are shown in figure.34:

Figure 34-Response of hot-pressed sample

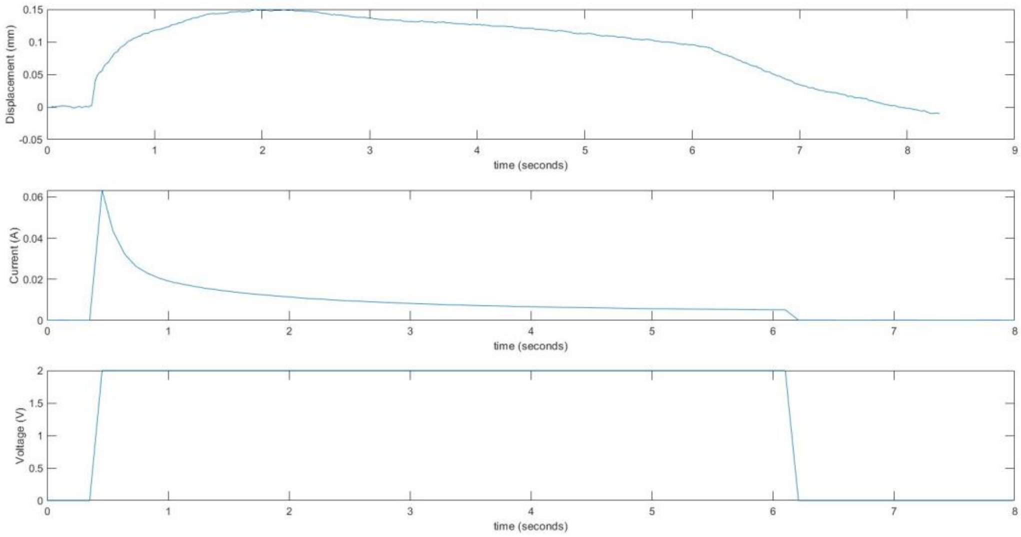

The difference in stiffness was evident between the sample when examining the data of the displacement sensor. The lowest stiffness was that of the hot-pressed membrane since it was the thinnest (0.2 mm). The sensor recorded high oscillations and fluctuations and was challenging to calibrate to a reference zero. This was also the case, although less severely, when calibrating the 3D-printed sample. The 3D printed sample with DAP presented very minimal oscillation due to external noise and perturbation, due to its significantly larger stiffness.

The results of the actuation along with the strains obtained are displayed in table.5 Below:

Table 5-Displacement results

Method	Max displacement (mm)	free length	thickness	strain
3D printed	0.285	10	0.4	0.00114
3D printed-DAP	0.0264	8	0.9	0.00037125
3D printed reference	0.85	22	0.5	0.000878

Hot pressed	0.15	19	0.2	8.31025-05

Note that the results from reference [20] are taken at the lowest frequency (a period of longer than 10 seconds) and correspond to an applied signal of 2 Volts

The strain was computed using the following equation taken from [19]:

$$S = \frac{Dt}{L^2} \quad \textbf{(eq.25)}$$

Where D is the displacement (mm) t is the approximate thickness(mm) and L is the free length in a cantilever configuration (mm)

The specific capacity was also computed based on the current signal recorded. First, the charge is computed by integrating the current over time based on equation.26:

$$Q = \int_{t1}^{t2} I dt \quad \textbf{(eq.26)}$$

The trapezoidal method was chosen since it has an error of the order $O(h^2)$ with the formula shown in equation.27:

$$Q = 0.5 \times \Delta t \times \left(I(1) + I(n) + 2\sum_{j=2}^{n-1} I(j)\right) + O(\Delta t^2) \quad \textbf{(eq.27)}$$

$$Q \approx 0.5 \times \Delta t \times \left(I(1) + I(n) + 2\sum_{j=2}^{n-1} I(j)\right)$$

However, this method requires constant intervals in time. The current values were interpolated in Matlab using the function “interp1”, which return a linear interpolation between the points. To guarantee a low error rate, 500 points were used which resulted in a change of time below 0.05 seconds between the points for all cases.

The capacity is obtained by using equation.28:

$$C = \frac{Q}{V} \quad \textbf{(eq.28)}$$

The specific capacity can be obtained by dividing by the surface area computed from equation.29:

$$A = width \times length \quad \textbf{(eq.29)}$$

The results are shown in table.6:

Table 6-Specifc capacity results

	Q (Ah)	V(votls)	C(F)	Width(m)	Length(m)	C/m2
3D printed	1.86389E-05	2	9.32E-06	0.0028	0.0125	0.26627
3D printed-DAP	3.7293e-06	2	2.06E-06	0.003	0.0115	0.054047
Hot-pressed	1.78333E-05	2	8.92E-06	0.008	0.022	0.050663

The DAP based method was expected to have a higher specific capacity as demonstrated in previous studies [19]. This is due to damage to the electrode during the experiment and issues with mixing of the polymer-metal composites.

In addition to the unsuccessful plating of the hot-pressed version of the DAP, the plating of the 3D printed-DAP based sample took longer than other samples. After 4 plating rounds, the conductivity was still above 10 Ω/cm. This was not the case in the regular 3D printed sample, indicating early issue of platinum penetration.

In addition, the electrode were suffering from flaking cutting the sample. Adding on top of it multiple rounds of testing, the electrodes were not in a good state and do not represent the full potential of the solution.

Nonetheless, the DAP-3D printed sample still outperformed the hot-pressed sample. The regular 3D-printed sample achieved better strain and specific capacity compared to the one in [20]. This might be due to the filament formation which was conducted at a significantly lower temperature (200°C) compared to their experiments

(285°C). This leads to lower polymer degradation. In addition, the 3D printer was operating at lower temperatures (265°C) and much lower speeds also inducing less degradation due to shear and friction.

CHAPTER FIVE

CONCLUSION

3D printing the electrodes of an IPMC was investigated, inspired from the DAP process. The mixing process, filament fabrication, 3D printer set up and printing settings are all adjusted for the production of Nafion filaments and Nafion-Ruthenium Dioxide filaments

Homogenous mixing with the current methods and materials used was poor in general. Coupled with the high anisotropy of 3D printing, it resulted in a poor performance of the actuator. This was evident from the obstacles and slow plating process, microscope imaging and the below par displacement obtained at the end.

Nonetheless the method is implementable and provide great flexibility in design if the proper equipment is used. It could be a great asset when designing with patterned electrodes

FUTURE WORK

The mixed results obtained in this study highlight key areas that can be improved on for the future. The mixing method is the primary issue to fix. Looking at the extrusion results from [52], DMF could be used to dissolve the Nafion and Ruthenium Dioxide can be added and mixed more easily. The stability of Ruthenium Dioxide in DMF should be addressed first but solution mixing would provide more homogeneity for the solution and require lower extrusion temperatures.

Another aspect that can be improved on is the choice of 3D printer used. While the ender 3 is very flexible with an abundance of parts and open-source firmware, it is limited in terms of the quality and precision it can provide. A more precise 3D printer with very close tolerances in terms of motion would facilitate 3D printing smaller electrodes in terms of thickness. In addition, the nozzle of the extruder can be designed or chosen to produce less back pressure. A custom 3D printer would be significantly more expensive but provides higher precision and more control of the entire manufacturing process.

Lastly, a new design for a filament extruder can be investigated. Looking at the success of the current design in mitigating and eliminating die swell in some cases, an upgraded design would allow continuous filament fabrication and the production of Nafion spools instead of short filaments.

REFERENCES

[1] Z. X. Khoo et al., “3D printing of smart materials: A review on recent progresses in 4D printing,” Virtual and Physical Prototyping, vol. 10, no. 3, pp. 103–122, Jul. 2015, doi: 10.1080/17452759.2015.1097054.

[2] A. A. Basheer, “Advances in the smart materials applications in the aerospace industries,” AEAT, vol. 92, no. 7, pp. 1027–1035, Jun. 2020, doi: 10.1108/AEAT-02-2020-0040.

[3] V. Lopes Junior, V. Steffen, and M. A. Savi, Eds., Dynamics of Smart Systems and Structures: Concepts and Applications. Cham: Springer International Publishing, 2016. doi: 10.1007/978-3-319-29982-2.

[4] M. Su and Y. Song, “Printable Smart Materials and Devices: Strategies and Applications,” Chem. Rev., vol. 122, no. 5, pp. 5144–5164, Mar. 2022, doi: 10.1021/acs.chemrev.1c00303.

[5] D. M. Addington and D. L. Schodek, Smart materials and new technologies: for the architecture and design professions. Amsterdam ; Boston: Architectural Press, 2005.

[6] S. Bahl, H. Nagar, I. Singh, and S. Sehgal, “Smart materials types, properties and applications: A review,” Materials Today: Proceedings, vol. 28, pp. 1302–1306, 2020, doi: 10.1016/j.matpr.2020.04.505.

[7] R. Bogue, “Smart materials: a review of recent developments,” Assembly Automation, vol. 32, no. 1, pp. 3–7, Feb. 2012, doi: 10.1108/01445151211198674.

[8] Sweeney, W. A., Bryan, P. F., & BTX, P. Kirk-Othmer Encyclopedia of Chemical Technology, 2007.

[9] R. Bogue, “Smart materials: a review of capabilities and applications,” Assembly Automation, vol. 34, no. 1, pp. 16–22, Jan. 2014, doi: 10.1108/AA-10-2013-094.

[10] Y. Bar-Cohen, “Electroactive Polymers as Artificial Muscles: A Review,” Journal of Spacecraft and Rockets, vol. 39, no. 6, pp. 822–827, Nov. 2002, doi: 10.2514/2.3902.

[11] B. Bhandari, G.-Y. Lee, and S.-H. Ahn, “A review on IPMC material as actuators and sensors: Fabrications, characteristics and applications,” Int. J. Precis. Eng. Manuf., vol. 13, no. 1, pp. 141–163, Jan. 2012, doi: 10.1007/s12541-012-0020-8.

[12] K. J. Kim, W. Yim, J. W. Paquette, and D. Kim, “Ionic Polymer-metal Composites for Underwater Operation,” Journal of Intelligent Material Systems and Structures, vol. 18, no. 2, pp. 123–131, Feb. 2007, doi: 10.1177/1045389X06063468.

[13]W. Yim, J. Lee, and K. J. Kim, “An artificial muscle actuator for biomimetic underwater propulsors,” Bioinspir. Biomim., vol. 2, no. 2, pp. S31–S41, Jun. 2007, doi: 10.1088/1748-3182/2/2/S04.

[14]J. D. Carrico, T. Hermans, K. J. Kim, and K. K. Leang, "3D-Printing and Machine Learning Control of Soft Ionic Polymer-Metal Composite Actuators," Sci Rep, vol. 9, no. 1, p. 17482, Dec. 2019, doi: 10.1038/s41598-019-53570-y.

[15] Zheng Chen, S. Shatara, and Xiaobo Tan, "Modeling of Biomimetic Robotic Fish Propelled by An Ionic Polymer–Metal Composite Caudal Fin," IEEE/ASME Trans. Mechatron., vol. 15, no. 3, pp. 448–459, Jun. 2010, doi: 10.1109/TMECH.2009.2027812.

[16] J. Najem, S. A. Sarles, B. Akle, and D. J. Leo, "Biomimetic jellyfish-inspired underwater vehicle actuated by ionic polymer metal composite actuators," Smart Mater. Struct., vol. 21, no. 9, p. 094026, Sep. 2012, doi: 10.1088/0964-1726/21/9/094026.

[17] J. Brufau-Penella, M. Puig-Vidal, P. Giannone, S. Graziani, and S. Strazzeri, "Characterization of the harvesting capabilities of an ionic polymer metal composite device," Smart Mater. Struct., vol. 17, no. 1, p. 015009, Feb. 2008, doi: 10.1088/0964-1726/17/01/015009.

[18] B.-K. Fang, M.-S. Ju, and C.-C. K. Lin, "A new approach to develop ionic polymer–metal composites (IPMC) actuator: Fabrication and control for active catheter systems," Sensors and Actuators A: Physical, vol. 137, no. 2, pp. 321–329, Jul. 2007, doi: 10.1016/j.sna.2007.03.024.

[19] B. J. Akle, K. B. Wiles, D. J. Leo, and J. E. McGrath, "Effects of electrode morphology on the performance of BPSH and PATS ionic polymer transducers," presented at the Smart Structures and Materials, San Diego, CA, Jul. 2004, p. 413. doi: 10.1117/12.539528.

[20] J. D. Carrico, N. W. Traeden, M. Aureli, and K. K. Leang, "Fused filament 3D printing of ionic polymer-metal composites (IPMCs)," Smart Mater. Struct., vol. 24, no. 12, p. 125021, Dec. 2015, doi: 10.1088/0964-1726/24/12/125021.

[21] S. J. Lee, M. J. Han, S. J. Kim, J. Y. Jho, H. Y. Lee, and Y. H. Kim, "A new fabrication method for IPMC actuators and application to artificial fingers," Smart Mater. Struct., vol. 15, no. 5, pp. 1217–1224, Oct. 2006, doi: 10.1088/0964-1726/15/5/008.

[22] P. G. de Gennes, K. Okumura, M. Shahinpoor, and K. J. Kim, "Mechanoelectric effects in ionic gels," Europhys. Lett., vol. 50, no. 4, pp. 513–518, May 2000, doi: 10.1209/epl/i2000-00299-3.

[23] M. Shahinpoor, and K. J. Kim, "Experimental Study of Ionic Polymer-Metal Composites in Various Cation Forms: Actuation Behavior," Science and Engineering of Composite Materials, vol. 10, no. 6, pp. 423–436, Dec. 2002, doi: 10.1515/SECM.2002.10.6.423.

[24] V. Palmre et al., "An IPMC-enabled bio-inspired bending/twisting fin for underwater applications," Smart Mater. Struct., vol. 22, no. 1, p. 014003, Jan. 2013, doi: 10.1088/0964-1726/22/1/014003.

[25] T. Stalbaum, S. E. Nelson, V. Palmre, and K. J. Kim, "Multi degree of freedom IPMC sensor," presented at the SPIE Smart Structures and Materials + Nondestructive

Evaluation and Health Monitoring, San Diego, California, USA, Mar. 2014, p. 90562J. doi: 10.1117/12.2045671.

[26] M. A. Tsugawa, V. Palmre, J. D. Carrico, K. J. Kim, and K. K. Leang, “Slender tube-shaped and square rod-shaped IPMC actuators with integrated sensing for soft mechatronics,” Meccanica, vol. 50, no. 11, pp. 2781–2795, Nov. 2015, doi: 10.1007/s11012-015-0218-9.

[27] B. Kim et al., “Analysis of mechanical characteristics of the ionic polymer metal composite (IPMC) actuator using cast ion-exchange film,” presented at the Smart Structures and Materials, San Diego, CA, Jul. 2003, p. 486. doi: 10.1117/12.484296.

[28] K. J. Kim and M. Shahinpoor, “A novel method of manufacturing three-dimensional ionic polymer±metal composites (IPMCs) biomimetic sensors, actuators and arti®cial muscles,” p. 6, 2002.

[29] S. Trabia, Comprehensive Study of Spray-Painting and 3D Printing Fabrication Methods for Nafion® and Nafion® Equivalents in Ionic Polymermetal Composite Actuators and Sensors." Order No. 10825432, University of Nevada, Las Vegas, Ann Arbor, 2018

[30] R. B. Moore, K. M. Cable, and T. L. Croley, “Barriers to flow in semicrystalline ionomers. A procedure for preparing melt-processed perfluorosulfonate ionomer films and membranes,” Journal of Membrane Science, vol. 75, no. 1–2, pp. 7–14, Dec. 1992, doi: 10.1016/0376-7388(92)80002-2.

[31] Nelson, S. E., “Feasibility study of custom manufacturing methods of ionic polymer-metal composite sensors”, PhDT, 2015.

[32]S. Mbarek, N. El Kissi, Z. Baccouch, and C. Iojoiu, “Extrusion of Nafion and Aquivion membranes: environmentally friendly procedure and good conductivities,” Polym. Bull., vol. 76, no. 3, pp. 1151–1166, Mar. 2019, doi: 10.1007/s00289-018-2427-6.

[33] J. H. Park, S. W. Lee, D. S. Song, and J. Y. Jho, “Highly enhanced force generation of ionic polymer–metal composite actuators via thickness manipulation,” ACS Applied Materials & Interfaces, vol. 7, no. 30, pp. 16659–16667, 2015.

[34] S. Trabia, Z. Olsen, and K. J. Kim, “Searching for a new ionomer for 3D printable ionic polymer–metal composites: Aquivion as a candidate,” Smart Mater. Struct., vol. 26, no. 11, p. 115029, Nov. 2017, doi: 10.1088/1361-665X/aa919f.

[35] M. Shahinpoor and K. J. Kim, “Mass Transfer Induced Hydraulic Actuation in Ionic Polymer-Metal Composites,” Journal of Intelligent Material Systems and Structures, vol. 13, no. 6, pp. 369–376, Jun. 2002, doi: 10.1177/104538902761696715.

[36] W. Grot, Fluorinated Ionomers, Chadds Ford, Pennsylvania: William Andrew-Elsevier, 2011.

[37] C. K. Chung, P. K. Fung, Y. Z. Hong, M. S. Ju, C. C. K. Lin, and T. C. Wu, “A novel fabrication of ionic polymer-metal composites (IPMC) actuator with silver nano-

powders," Sensors and Actuators B: Chemical, vol. 117, no. 2, pp. 367–375, Oct. 2006, doi: 10.1016/j.snb.2005.11.021.

[38] S.-M. Kim and K. J. Kim, "Palladium buffer-layered high performance ionic polymer–metal composites," Smart Mater. Struct., vol. 17, no. 3, p. 035011, Jun. 2008, doi: 10.1088/0964-1726/17/3/035011.

[39] V. Palmre et al., "Electroactive polymer actuators with carbon aerogel electrodes," J. Mater. Chem., vol. 21, no. 8, p. 2577, 2011, doi: 10.1039/c0jm01729a.

[40] Tiwari, R., & Garcia, E. (2011). The state of understanding of ionic polymer metal composite architecture: a review. Smart Materials and Structures, 20(8), 083001.

[41] Oguro, K., Fujiwara, N., Asaka, K., Onishi, K., & Sewa, S. (1999, May). Polymer electrolyte actuator with gold electrodes. In Smart Structures and Materials 1999: Electroactive Polymer Actuators and Devices (Vol. 3669, pp. 64-71). SPIE.

[42] Nemat-Nasser, S. (2002). Micromechanics of actuation of ionic polymer-metal composites. Journal of applied Physics, 92(5), 2899-2915.

[43] Leo, D. J., Farinholt, K., & Wallmersperger, T. (2005, May). Computational models of ionic transport and electromechanical transduction in ionomeric polymer transducers. In Smart Structures and Materials 2005: Electroactive Polymer Actuators and Devices (EAPAD) (Vol. 5759, pp. 170-181). SPIE

[44] Akle, B. J., Leo, D. J., Hickner, M. A., & McGrath, J. E. (2005). Correlation of capacitance and actuation in ionomeric polymer transducers. Journal of Materials Science, 40(14), 3715–3724. https://doi.org/10.1007/s10853-005-3312-x

[45] Akle, B. J., Bennett, M. D., Leo, D. J., Wiles, K. B., & McGrath, J. E. (2007). Direct assembly process: A novel fabrication technique for large strain ionic polymer transducers. Journal of Materials Science, 42(16), 7031–7041. https://doi.org/10.1007/s10853-006-0632-4

[46] Shahinpoor, M., & Kim, K. J. (2000). The effect of surface-electrode resistance on the performance of ionic polymer-metal composite (IPMC) artificial muscles. Smart Materials and Structures, 9(4), 543.

[47] Shahinpoor, M., & Kim, K. J. (2001). Ionic polymer-metal composites: I. Fundamentals. Smart materials and structures, 10(4), 819.

[48] Millet, P., Durand, R., Dartyge, E., Tourillon, G., & Fontaine, A. (1993). Precipitation of metallic platinum into Nafion ionomer membranes: I . Experimental results. Journal of The Electrochemical Society, 140(5), 1373-1380. doi:DOI:10.1149/1.2221563

[49] Kim, K. J., & Shahinpoor, M. (2003). Ionic polymer–metal composites: II. Manufacturing techniques. Smart materials and structures, 12(1), 65.

[50] Pak, J. J., Cha, S. E., Ahn, H. J., & Lee, S. K. (2001). Fabrication of ionic polymer metal composites by electroless plating of platinum. In Proceedings of the 32nd ISR (International Symposium on Robotics).

[51] Shahinpoor, M., & Kim, K. J. (2002). Novel ionic polymer–metal composites equipped with physically loaded particulate electrodes as biomimetic sensors, actuators and artificial muscles. Sensors and Actuators A: Physical, 96(2-3), 125-132.

[52] Wang, H. S., Cho, J., Song, D. S., Jang, J. H., Jho, J. Y., & Park, J. H. (2017). High-performance electroactive polymer actuators based on ultrathick ionic polymer–metal composites with nanodispersed metal electrodes. ACS applied materials & interfaces, 9(26), 21998-22005.

[53] Bhaskar, S., Dobal, P. S., Majumder, S. B., & Katiyar, R. S. (2000). Characterization of Conductive RuO2 Thin Film as Bottom electrodes for Ferroelectric Thin Films. MRS Online Proceedings Library (OPL), 655.

[54]Akle, B. J., Bennett, M. D., & Leo, D. J. (2006). High-strain ionomeric–ionic liquid electroactive actuators. Sensors and Actuators A: Physical, 126(1), 173–181. https://doi.org/10.1016/j.sna.2005.09.006

[55] Akle, B., Nawshin, S., & Leo, D. (2007). Reliability of high strain ionomeric polymer transducers fabricated using the direct assembly process. Smart Materials and Structures, 16(2), S256–S261. https://doi.org/10.1088/0964-1726/16/2/S09

[56] Supriya, L., Akle, B. J., Leo, D. J., & Claus, R. O. (2007). Assembly of Au electrodes on polymeric sensors and actuators using a poly (urethane urea) linking agent. IEEE Sensors J.

[57] Griffiths, D., Sundaresan, V. B., Akle, B., Vlachos, P., & Leo, D. (2008). Micro deposition method: A novel fabrication method for Ionic polymer metallic composites. *SPIE-Electroactive Polymer Actuators and Devices (EAPAD), 6927*. doi:https://doi.org/10.1117/12.776462

[58] Tang, W., Zhang, R., Liu, B., & Yuan, H. (2014). Perfluorosulfonated ionomers membranes: Melt-processing and characterization for ion exchange applications. Journal of Applied Polymer Science, 131(4), n/a-n/a. https://doi.org/10.1002/app.39944

[59] Trabia, S., Choi, K., Olsen, Z., Hwang, T., Nam, J.-D., & Kim, K. (2018). Understanding the Thermal Properties of Precursor-Ionomers to Optimize Fabrication Processes for Ionic Polymer-Metal Composites (IPMCs). Materials, 11(5), 665. https://doi.org/10.3390/ma11050665

[60] Bellini, A., Gu¨ c¸ eri, S. U., & Bertoldi, M. (2004). Liquefier dynamics in fused deposition. J. Manuf. Sci. Eng., 126(2), 237-246.

[61] De Almeida, S., & Kawano, Y. (1999). Thermal behavior of Nafion membranes. Journal of Thermal Analysis and Calorimetry, 58(3), 569-577.

[62] Luan, Y., Zhao, J., Yang, J., & Ma, X. (2012). Thermal analysis of perfluorosulfonated ionomers. Journal of Thermal Analysis and Calorimetry, 110(3), 1119–1126. https://doi.org/10.1007/s10973-011-2020-9

[63] O'Neill, M. J. (1966). Measurement of Specific Heat Functions by Differential Scanning Calorimetry. Analytical Chemistry, 38(10), 1331–1336. https://doi.org/10.1021/ac60242a011

[64]Mauritz, K. A., & Moore, R. B. (2004). State of Understanding of Nafion. Chemical Reviews, 104(10), 4535–4586. https://doi.org/10.1021/cr0207123

[65] Elliott, J. A., James, P. J., McMaster, T. J., Newton, J. M., Elliott, A. M. S., Hanna, S., & Miles, M. J. (2001). Hydrolysis of the Nafion® precursor studied by X-ray scattering and in-situ atomic force microscopy. E-Polymers, 1(1). https://doi.org/10.1515/epoly.2001.1.1.210

[66] Liang, J. Z., Li, R. K. Y., Tang, C. Y., & Cheung, S. W. (2000). Die–swell behavior of glass bead-filled low-density polyethylene composite melts at high extrusion rates. Journal of applied polymer science, 76(3), 419-424

[67] Tanner, R. I. (1970). A theory of die-swell. Journal of Polymer Science Part A-2: Polymer Physics, 8(12), 2067–2078. https://doi.org/10.1002/pol.1970.160081203

[68] Larson, R. G. (2013). Constitutive equations for polymer melts and solutions: Butterworths series in chemical engineering. Butterworth-Heinemann.

[69] Henderson, A. M., & Rudin, A. (1986). Effects of die temperature on extrudate swell in screw extrusion. Journal of Applied Polymer Science, 31(2), 353–365. https://doi.org/10.1002/app.1986.070310206

[70] Nielsen, L. E. Polymer rheology. 1977, New York: M. Dekker, 47, 1145-1149.

[71] Haworth, B., Gilbert, M., & Myers, D. J. B. (2005). Melt-state shear flow and elasticity of a thermoplastic fluorosulphonated—PTFE copolymer. Journal of Materials Science, 40(4), 955–964. https://doi.org/10.1007/s10853-005-6514-3

[72] Minagawa, N., & White, J. L. (1976). The influence of titanium dioxide on the rheological and extrusion properties of polymer melts. Journal of applied polymer science, 20(2), 501-523.

[73] Turner, B. N., Strong, R., & Gold, S. A. (2014). A review of melt extrusion additive manufacturing processes: I. Process design and modeling. Rapid prototyping journal.

[74] Rosenzweig, N., & Narkis, M. (1981). Sintering rheology of amorphous polymers. Polymer Engineering & Science, 21(17), 1167-1170.

[75] Zhang, X., & Wang, J. (2020). Controllable interfacial adhesion behaviors of polymer-on-polymer surfaces during fused deposition modeling 3D printing process. Chemical Physics Letters, 739, 136959. https://doi.org/10.1016/j.cplett.2019.136959

[76] Alafaghani, A., Qattawi, A., Alrawi, B., & Guzman, A. (2017). Experimental Optimization of Fused Deposition Modelling Processing Parameters: A Design-for-Manufacturing Approach. Procedia Manufacturing, 10, 791–803. https://doi.org/10.1016/j.promfg.2017.07.079

[77] Venkataraman, N., Rangarajan, S., Matthewson, M. J., Safari, A., Danforth, S. C., Yardimci, A., & Guceri, S. I. (1999). Mechanical and rheological properties of feedstock material for fused deposition of ceramics and metals (FDC and FDMet) and their relationship to process performance. In 1999 International Solid Freeform Fabrication Symposium.

[78] Elbadawi, M., Rivera-Armenta, J. L., & Cruz, B. A. S. (2018). Polymeric additive manufacturing: the necessity and utility of rheology. Polymer Rheology, 10, 43.

[79] Carrico, J. D., Erickson, J. M., & Leang, K. K. (2016, April). Characterization of 3D-printed IPMC actuators. In Electroactive Polymer Actuators and Devices (EAPAD) 2016 (Vol. 9798, pp. 427-434). SPIE.

[80] Bertolino, M., Battegazzore, D., Arrigo, R., & Frache, A. (2021). Designing 3D printable polypropylene: Material and process optimisation through rheology. Additive Manufacturing, 40, 101944. https://doi.org/10.1016/j.addma.2021.101944

[81] Yin, J., Lu, C., Fu, J., Huang, Y., & Zheng, Y. (2018). Interfacial bonding during multi-material fused deposition modeling (FDM) process due to inter-molecular diffusion. Materials & Design, 150, 104-112.

[82] Maeda, N., Chen, N., Tirrell, M., & Israelachvili, J. N. (2002). Adhesion and friction mechanisms of polymer-on-polymer surfaces. Science, 297(5580), 379-382.

[83] Jang, S., Boddorff, A., Jang, D. J., Lloyd, J., Wagner, K., Thadhani, N., & Brettmann, B. (2021). Effect of material extrusion process parameters on filament geometry and inter-filament voids in as-fabricated high solids loaded polymer composites. Additive Manufacturing, 47, 102313. https://doi.org/10.1016/j.addma.2021.102313

[84] Valkenaers, H., Vogeler, F., Voet, A., & Kruth, J. P. (2013). Screw extrusion based 3D printing, a novel additive manufacturing technology. In Proceedings of the 5th international conference on competitive manufacturing (pp. 97-103). University of Stellenbosch; Stellenbosch.

[85] Ramanath, H. S., Chua, C. K., Leong, K. F., & Shah, K. D. (2008). Melt flow behaviour of poly-ε-caprolactone in fused deposition modelling. Journal of Materials Science: Materials in Medicine, 19(7), 2541-2550.

[86] Park, S., & Fu, K. (Kelvin). (2021). Polymer-based filament feedstock for additive manufacturing. Composites Science and Technology, 213, 108876. https://doi.org/10.1016/j.compscitech.2021.108876

[87] Ryder, M. A., Lados, D. A., Iannacchione, G. S., & Peterson, A. M. (2018). Fabrication and properties of novel polymer-metal composites using fused deposition

modeling. Composites Science and Technology, 158, 43–50. https://doi.org/10.1016/j.compscitech.2018.01.049

[88] Amir Mostafapour. (2012). A study on the role of processing parameters in joining polyethylene sheets via heat assisted friction stir welding: Investigating microstructure, tensile and flexural properties. International Journal of the Physical Sciences, 7(4). https://doi.org/10.5897/IJPS11.1653

[89] Berretta, S., Davies, R., Shyng, Y. T., Wang, Y., & Ghita, O. (2017). Fused Deposition Modelling of high temperature polymers: Exploring CNT PEEK composites. Polymer Testing, 63, 251-262.

[90] Hasib, A. G., Niauzorau, S., Xu, W., Niverty, S., Kublik, N., Williams, J., Chawla, N., Song, K., & Azeredo, B. (2021). Rheology scaling of spherical metal powders dispersed in thermoplastics and its correlation to the extrudability of filaments for 3D printing. Additive Manufacturing, 41, 101967. https://doi.org/10.1016/j.addma.2021.101967

[91] Gonzalez-Gutierrez, J., Duretek, I., Arbeiter, F., Kukla, C., & Holzer, C. (2017, May). Filler content and properties of highly filled filaments for fused filament fabrication of magnets. In SPE ANTEC 2017.

[92] Geus, H. G. (2016). Developments in manufacturing techniques for technical nonwovens. In Advances in Technical Nonwovens (pp. 133-153). Woodhead Publishing

[93] Vlachopoulos, J., & Strutt, D. (2003). Polymer processing. Materials science and technology, 19(9), 1161-1169.

[94] Tan, D. K., Maniruzzaman, M., & Nokhodchi, A. (2018). Advanced pharmaceutical applications of hot-melt extrusion coupled with fused deposition modelling (FDM) 3D printing for personalised drug delivery. Pharmaceutics, 10(4), 203

[95] Nabipour, M., Akhoundi, B., & Saed, A. B. (2020). Manufacturing of polymer/metal composites by fused deposition modeling process with polyethylene. J. APPL. POLYM. SCI., 9.

[96] Strano, M., Rane, K., Briatico Vangosa, F., & Di Landro, L. (2019). Extrusion of metal powder-polymer mixtures: Melt rheology and process stability. Journal of Materials Processing Technology, 273, 116250. https://doi.org/10.1016/j.jmatprotec.2019.116250

[97] Mannschatz, A., Müller, A., & Moritz, T. (2011). Influence of powder morphology on properties of ceramic injection moulding feedstocks. Journal of the European Ceramic Society, 31(14), 2551-2558.

[98] Fereiduni, E., Ghasemi, A., & Elbestawi, M. (2019). Characterization of composite powder feedstock from powder bed fusion additive manufacturing perspective. Materials, 12(22), 3673.

[99] Roberson, D., Shemelya, C. M., MacDonald, E., & Wicker, R. (2015). Expanding the applicability of FDM-type technologies through materials development. Rapid Prototyping Journal.

[100] Boparai, K. S., Singh, R., & Singh, H. (2016). Development of rapid tooling using fused deposition modeling: a review. Rapid Prototyping Journal, 22(2), 281-299.

[101] Wang, X., Jiang, M., Zhou, Z., Gou, J., & Hui, D. (2017). 3D printing of polymer matrix composites: A review and prospective. Composites Part B: Engineering, 110, 442-458.

[102] Mackay, M. E. (2018). The importance of rheological behavior in the additive manufacturing technique material extrusion. Journal of Rheology, 62(6), 1549-1561.

[103] Torrado Perez, A. R., Roberson, D. A., & Wicker, R. B. (2014). Fracture Surface Analysis of 3D-Printed Tensile Specimens of Novel ABS-Based Materials. Journal of Failure Analysis and Prevention, 14(3), 343–353. https://doi.org/10.1007/s11668-014-9803-9

[104] Hwang, S., Reyes, E. I., Moon, K., Rumpf, R. C., & Kim, N. S. (2015). Thermo-mechanical Characterization of Metal/Polymer Composite Filaments and Printing Parameter Study for Fused Deposition Modeling in the 3D Printing Process. Journal of Electronic Materials, 44(3), 771–777. https://doi.org/10.1007/s11664-014-3425-6

[105] Woern, A. L., McCaslin, J. R., Pringle, A. M., & Pearce, J. M. (2018). RepRapable Recyclebot: Open source 3-D printable extruder for converting plastic to 3-D printing filament. HardwareX, 4, e00026.

[106] Spinelli, G., Kotsilkova, R., Ivanov, E., Petrova-Doycheva, I., Menseidov, D., Georgiev, V., ... & Silvestre, C. (2019). Effects of filament extrusion, 3D printing and hot-pressing on electrical and tensile properties of poly (lactic) acid composites filled with carbon nanotubes and graphene. Nanomaterials, 10(1), 35

[107] Goh, G. L., Agarwala, S., & Yeong, W. Y. (2019). Directed and on-demand alignment of carbon nanotube: a review toward 3D printing of electronics. Advanced Materials Interfaces, 6(4), 1801318.

[108] D. G. Alciatore and M. B. Histand, Introduction to mechatronics and measurement systems, 4th ed. New York: McGraw-Hill, 2012.

[109] R. Zheng, R. I. Tanner, and X.-J. Fan, Injection Molding. Berlin, Heidelberg: Springer Berlin Heidelberg, 2011. doi: 10.1007/978-3-642-21263-5.

[110] C. I. Chung, Extrusion of Polymers: Theory & Practice, 3rd ed. München: Carl Hanser Verlag GmbH & Co. KG, 2019. doi: 10.3139/9781569907382.

[111] C. Rauwendaal and P. J. Gramann, Polymer extrusion, 5. ed. Munich: Hanser, 2014.

[112] R. G. Larson, Constitutive Equations for Polymer Melts and Solutions, Butterworths Series in Chemical Engineering, 1988.